iScience

CellPress
OPEN ACCESS

Article

Experimental and natural evidence of SARS-CoV-2-infection-induced activation of type I interferon responses

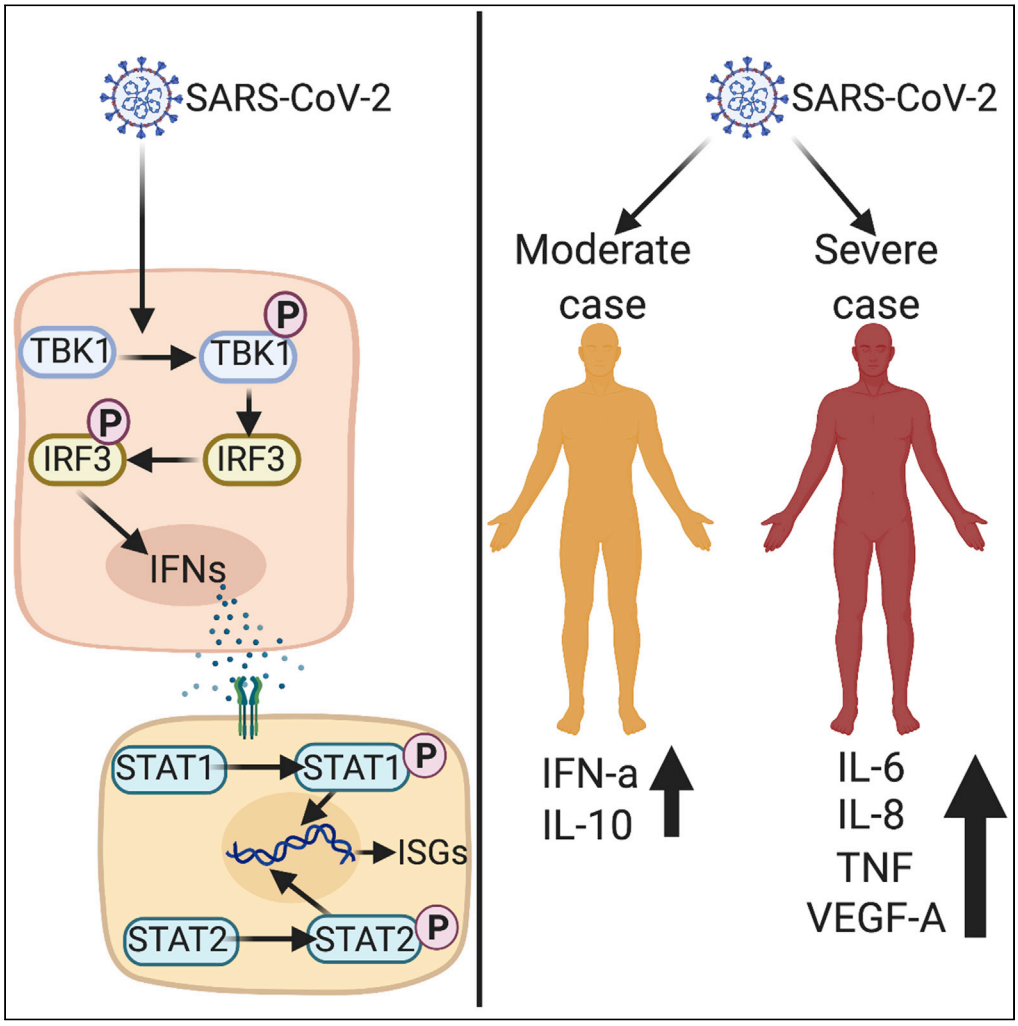

Arinjay Banerjee, Nader El-Sayes, Patrick Budylowski, ..., Andrew G. McArthur, Andrew C. Doxey, Karen Mossman

arinjay.banerjee@usask.ca (A.B.)
mossk@mcmaster.ca (K.M.)

Highlights

SARS-CoV-2 induces the expression of type I IFNs in human lung cells

Moderate cases of COVID-19 have higher serum levels of IL-10 and IFNα

Severe cases of COVID-19 have higher serum levels of IL-6, TNFα and IL-8

Physiological levels of IFNα reduces SARS-CoV-2 replication in human airway cells

Banerjee et al., iScience *24*, 102477
May 21, 2021
https://doi.org/10.1016/j.isci.2021.102477

iScience

CellPress
OPEN ACCESS

Article

Experimental and natural evidence of SARS-CoV-2-infection-induced activation of type I interferon responses

Arinjay Banerjee,[1,2,3,21,*] Nader El-Sayes,[3,4,22] Patrick Budylowski,[5,22] Rajesh Abraham Jacob,[1,2,3,22] Daniel Richard,[6,22] Hassaan Maan,[7,8] Jennifer A. Aguiar,[9] Wael L. Demian,[1,2,3] Kaushal Baid,[3,4] Michael R. D'Agostino,[2,3,4] Jann Catherine Ang,[2,3,4] Tetyana Murdza,[3,4] Benjamin J.-M. Tremblay,[9] Sam Afkhami,[2,3,4] Mehran Karimzadeh,[7] Aaron T. Irving,[11,12] Lily Yip,[13] Mario Ostrowski,[14,15] Jeremy A. Hirota,[2,16,17] Robert Kozak,[13,18] Terence D. Capellini,[6] Matthew S. Miller,[2,3,4] Bo Wang,[7,8,10,18] Samira Mubareka,[13,18] Allison J. McGeer,[19,20] Andrew G. McArthur,[2,4] Andrew C. Doxey,[2,9] and Karen Mossman[1,2,3,23,*]

SUMMARY

Type I interferons (IFNs) are our first line of defense against virus infection. Recent studies have suggested the ability of SARS-CoV-2 proteins to inhibit IFN responses. Emerging data also suggest that timing and extent of IFN production is associated with manifestation of COVID-19 severity. In spite of progress in understanding how SARS-CoV-2 activates antiviral responses, mechanistic studies into wild-type SARS-CoV-2-mediated induction and inhibition of human type I IFN responses are scarce. Here we demonstrate that SARS-CoV-2 infection induces a type I IFN response *in vitro* and in moderate cases of COVID-19. *In vitro* stimulation of type I IFN expression and signaling in human airway epithelial cells is associated with activation of canonical transcriptions factors, and SARS-CoV-2 is unable to inhibit exogenous induction of these responses. Furthermore, we show that physiological levels of IFNα detected in patients with moderate COVID-19 is sufficient to suppress SARS-CoV-2 replication in human airway cells.

INTRODUCTION

Severe acute respiratory syndrome coronavirus 2 (SARS-CoV-2) emerged in December 2019 to cause a global pandemic of coronavirus disease (COVID-19) (Zhou et al., 2020a). SARS-CoV-2 causes a respiratory infection, along with acute respiratory distress syndrome in severe cases. Innate antiviral responses, which include type I interferons (IFNs), are the first line of antiviral defense against an invading virus (Kawai and Akira, 2006). Cellular pattern recognition receptors (PRRs) recognize viral nucleic acids and activate key cellular kinases, such as inhibitor of nuclear factor kappa-B kinase subunit epsilon (IKKε) and TANK-binding kinase 1 (TBK1). These kinases phosphorylate and activate transcription factors such as interferon regulatory factor 3 (IRF3) to stimulate downstream production of type I/III IFNs (Koyama et al., 2008). Type I IFNs interact with interferon alpha/beta receptor (IFNAR) on cells to induce phosphorylation and activation of downstream mediators, such as signal transducer and activator of transcription 1 and 2 (STAT1 and STAT2), which leads to the production of antiviral interferon-stimulated genes (ISGs). Similarly, type III IFNs interact with their cognate receptors, IL-10R2 and IFNLR1, to activate STAT1 and STAT2, followed by the production of ISGs (Mesev et al., 2019).

Viruses encode proteins that can inhibit type I IFN production and signaling (Katze et al., 2002; Schulz and Mossman, 2016). Emerging pathogenic human coronaviruses, such as SARS-CoV and Middle East respiratory syndrome (MERS)-CoV, have evolved multiple proteins that inhibit type I IFN responses in human cells (Chen et al., 2014; de Wit et al., 2016; Lu et al., 2011; Siu et al., 2014; Yang et al., 2013). Thus, to better understand SARS-CoV-2 pathogenesis, it is critical to identify the dynamic interaction of SARS-CoV-2 and the type I IFN response. Emerging data suggest that ectopic expression of at least 13 SARS-CoV-2 proteins, namely NSP1, NSP3, NSP6, NSP12, NSP13, NSP14, NSP15, M, ORF3a, ORF6, ORF7a, ORF7b, and

[1]Department of Medicine, McMaster University, Hamilton, ON L8N 3Z5, Canada

[2]Michael G. DeGroote Institute for Infectious Disease Research, McMaster University, Hamilton, ON L8S 4K1, Canada

[3]McMaster Immunology Research Centre, McMaster University, Hamilton, ON L8S 4K1, Canada

[4]Department of Biochemistry and Biomedical Sciences, McMaster University, Hamilton, ON L8S 4K1, Canada

[5]Institute of Medical Science, University of Toronto, Toronto, ON M5S 1A8, Canada

[6]Department of Human Evolutionary Biology, Harvard University, Cambridge, MA 02138, USA

[7]Vector Institute for Artificial Intelligence, Toronto, ON M5G 1M1, Canada

[8]Peter Munk Cardiac Centre, University Health Network, Toronto, ON M5G 2C4, Canada

[9]Department of Biology, University of Waterloo, Waterloo, ON N2L 3G1, Canada

[10]Department of Computer Science, University of Toronto, Toronto, ON M5S 2E4, Canada

[11]Zhejiang University – University of Edinburgh Institute, Haining, Zhejiang 314400, China

Continued

ORF9b, can inhibit type I IFN responses in human cells (Gordon et al., 2020; Jiang et al., 2020; Lei et al., 2020; Xia et al., 2020). However, limited studies have captured the dynamic interplay of viral-RNA-mediated upregulation of type I IFN responses, followed by subsequent modulation of these responses by SARS-CoV-2 proteins as they accumulate in infected cells. Understanding the mechanisms of IFN modulation by SARS-CoV-2 proteins remains an area of intense research. In the meantime, intriguing observations about SARS-CoV-2 proteins have been reported by different groups. For example, SARS-CoV-2 NSP15 has been reported as an IFN-modulating protein by Gordon et al. (Gordon et al., 2020), but Lei et al. (Lei et al., 2020) were unable to identify NSP15 as an inhibitor of IFN promoter activation. In addition, both Gordon et al. and Jiang et al. identified ORF9b as a modulator of IFN responses (Gordon et al., 2020; Jiang et al., 2020; Lei et al., 2020), but the study by Lei et al. did not identify ORF9b as a modulator (Lei et al., 2020). Furthermore, infection with wild-type SARS-CoV-2 in Caco-2 cells activated phosphorylation of TBK1 and IRF3, along with mild induction of ISGs (Shin et al., 2020). More recently, Yin et al. have demonstrated that wild-type SARS-CoV-2 induces a delayed type I IFN response via melanoma differentiation-associated protein 5 (MDA5) recognition (Yin et al., 2021). Thus, in-depth studies with clinical isolates of SARS-CoV-2 are required to confidently identify type I IFN responses that are generated in infected human cells and to determine the dynamic induction and modulation of type I IFN responses by wild-type virus infection.

Transcriptional data from *in vitro* and *in vivo* work have demonstrated the lack of induction of type I IFN responses following SARS-CoV-2 infection (Blanco-Melo et al., 2020). In contrast, emerging data from patients with mild and moderate cases of COVID-19 have demonstrated the presence of type I IFN (Hadjadj et al., 2020a; Trouillet-Assant et al., 2020). Subsequently, recent studies have identified type I IFN responses in severe COVID-19 cases, which have been speculated to be associated with an exacerbated inflammatory response (Zhou et al., 2020b). In addition, upregulation of ISGs was also identified in a single-cell RNA sequencing study of peripheral blood mononuclear cells (PBMCs) from hospitalized COVID-19 patients (Wilk et al., 2020). Studies with patient samples are critical to understand the pathogenesis of SARS-CoV-2; however, the timing of sample collection, case definition of disease severity, and varying viral load can lead to different observations related to IFN responses. An early and controlled IFN response is preferable during virus infection. Excessive induction of type I IFN responses in COVID-19 patients is associated with higher levels of damaging inflammatory molecules (Lucas et al., 2020). Thus, it is critical to identify the extent to which SARS-CoV-2 can induce or inhibit human IFN responses using controlled mechanistic studies.

In this study, we have identified global early transcriptional responses that are initiated during infection of human airway epithelial (Calu-3) cells at 0, 1, 2, 3, 6, and 12 h post incubation with a clinical isolate of SARS-CoV-2 from a COVID-19 patient in Toronto (Banerjee et al., 2020a). Data from our study demonstrate that SARS-CoV-2 infection induces the expression of type I IFNs, along with the expression of downstream ISGs. We also identified an increasing trend for type I IFN expression (IFN-α2) in sera from moderate cases of COVID-19, relative to healthy individuals and severe cases of COVID-19. *In vitro* infection with SARS-CoV-2 induced phosphorylation of canonical transcription factors that are involved in the type I IFN response, such as IRF3, STAT1, and STAT2; exogenous activation of these transcription factors was not inhibited by wild-type SARS-CoV-2. In addition, we detected higher serum levels of anti-inflammatory cytokines in moderate cases of COVID-19 than in severe cases. Severe cases of COVID-19 displayed higher serum levels of pro-inflammatory cytokines. Data from our study suggest that replication-competent SARS-CoV-2 induces type I IFN responses in human airway epithelial cells, and type I IFN (IFN-α2) level detected in patients with moderate COVID-19 is sufficient to reduce SARS-CoV-2 replication in these cells. Further mechanistic studies are warranted to identify host factors (Bastard et al., 2020; Zhang et al., 2020) that contribute to varying disease severity during the course of COVID-19, along with the regulation of inflammatory and anti-inflammatory cellular processes in SARS-CoV-2-infected cells.

RESULTS

Global cellular response in SARS-CoV-2-infected human airway epithelial cells

The replication cycle of CoVs is complex and involves the generation of sub-genomic RNA molecules, which in turn code for mRNA that are translated into proteins (Banerjee et al., 2019; Sawicki et al., 2007). To determine SARS-CoV-2 replication kinetics in human cells using RNA sequencing (RNA-seq), we infected human airway epithelial cells (Calu-3) at a multiplicity of infection (MOI) of 2. After incubation with virus inoculum for 1 h, media was replaced with cell growth media and RNA was extracted and

[12]Second Affiliated Hospital, Zhejiang University School of Medicine, Hangzhou 310027, China

[13]Sunnybrook Research Institute, Toronto, ON M4N 3M5, Canada

[14]Department of Medicine, University of Toronto, Toronto, ON M5S 3H2, Canada

[15]Keenan Research Centre for Biomedical Science of St. Michael's Hospital, UnityHealth, Toronto, ON M5B 1W8, Canada

[16]Division of Respirology, Department of Medicine, McMaster University, Hamilton, ON L8N 3Z5, Canada

[17]Division of Respiratory Medicine, The University of British Columbia, Vancouver, BC V5Z 1M9, Canada

[18]Department of Laboratory Medicine and Pathobiology, University of Toronto, Toronto, ON M5S 1A8, Canada

[19]Mount Sinai Hospital, Toronto, ON M5G 1X5, Canada

[20]Dalla Lana School of Public Health, University of Toronto, Toronto, ON M5S 1A1, Canada

[21]Present address: Vaccine and Infectious Disease Organization, Department of Veterinary Microbiology, University of Saskatchewan; Saskatoon, SK S7N 5E3, Canada

[22]These authors contributed equally

[23]Lead contact

*Correspondence: arinjay.banerjee@usask.ca (A.B.), mossk@mcmaster.ca (K.M.)

https://doi.org/10.1016/j.isci.2021.102477

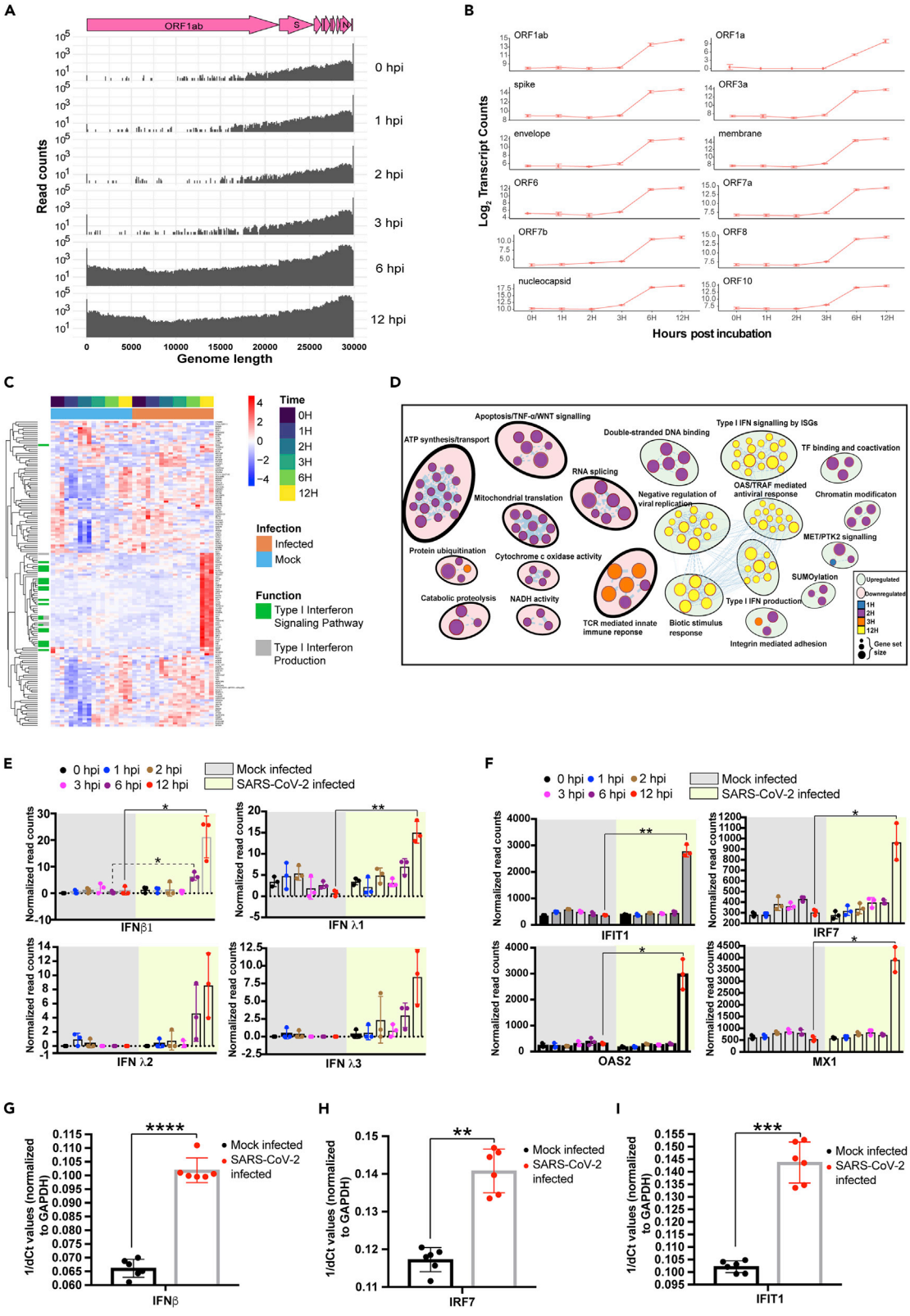
A
ORF1ab
S
N
0 hpi
1 hpi
2 hpi
3 hpi
6 hpi
12 hpi
Read counts
Genome length
B
ORF1ab
ORF1a
spike
ORF3a
envelope
membrane
ORF6
ORF7a
ORF7b
ORF8
nucleocapsid
ORF10
Log2 Transcript Counts
Hours post incubation
C
Time
0H
1H
2H
3H
6H
12H
Infection
Infected
Mock
Function
Type I Interferon Signaling Pathway
Type I Interferon Production
D
Apoptosis/TNF-α/WNT signalling
ATP synthesis/transport
Double-stranded DNA binding
Type I IFN signalling by ISGs
TF binding and coactivation
RNA splicing
Mitochondrial translation
Negative regulation of viral replication
OAS/TRAF mediated antiviral response
Chromatin modificaton
MET/PTK2 signalling
Protein ubiquitination
Cytochrome c oxidase activity
SUMOylation
Catabolic proteolysis
NADH activity
Type I IFN production
TCR mediated innate immune reponse
Biotic stimulus response
Integrin mediated adhesion
Upregulated
Downregulated
1H
2H
3H
12H
Gene set size
E
0 hpi 1 hpi 2 hpi
3 hpi 6 hpi 12 hpi
Mock infected
SARS-CoV-2 infected
Normalized read counts
IFNβ1
IFN λ1
IFN λ2
IFN λ3
F
0 hpi 1 hpi 2 hpi
3 hpi 6 hpi 12 hpi
Mock infected
SARS-CoV-2 infected
Normalized read counts
IFIT1
IRF7
OAS2
MX1
G
1/dCt values (normalized to GAPDH)
Mock infected
SARS-CoV-2 infected
IFNβ
H
1/dCt values (normalized to GAPDH)
Mock infected
SARS-CoV-2 infected
IRF7
I
1/dCt values (normalized to GAPDH)
Mock infected
SARS-CoV-2 infected
IFIT1

Figure 1. Global response in SARS-CoV-2-infected human airway epithelial cells

Calu-3 cells were infected with SARS-CoV-2 at an MOI of 1 or 2. RNA was extracted at different times post incubation. Viral and cellular gene expression was determined using time-series RNA-seq analysis or qPCR.

(A) SARS-CoV-2 gene expression over 12 h (n = 3/time point). The genome organization of SARS-CoV-2 is indicated above in pink.

(B) Major SARS-CoV-2 gene expression levels at different times post incubation (n = 3/time point).

(C) Cellular genes (n = 124) that are significantly up- or downregulated (FDR-adjusted p < 0.05; |log2FC| > 1) in SARS-CoV-2-infected cells, relative to mock-infected cells at different times post incubation. Transcript levels are shown as *Z* score normalized expression (scaled by gene). See Figure S1E for a larger figure.

(D) Cellular processes that are down- or upregulated at different times post incubation. The size of the circles represents the number of genes that are down- or upregulated at different times after incubation (n = 3/time point).

(E) Transcript abundance of type I and III interferon (IFN) genes (*IFNβ* and *IFNλ1-3*) in mock-infected and SARS-CoV-2-infected Calu-3 cells at different times (n = 3).

(F) Transcript abundance of representative interferon-stimulated genes (ISGs) in mock-infected and SARS-CoV-2-infected Calu-3 cells at different times (n = 3).

(G) *IFNβ* transcript levels in Calu-3 cells infected with SARS-CoV-2 or mock infected for 12 h, normalized to *GAPDH* (n = 6). Transcript levels were determined by qPCR.

(H) *IRF7* transcript levels in Calu-3 cells infected with SARS-CoV-2 or mock infected for 12 h, normalized to *GAPDH* (n = 6). Transcript levels were determined by qPCR.

(I) *IFIT1* transcript levels in Calu-3 cells infected with SARS-CoV-2 or mock infected for 12 h, normalized to *GAPDH* (n = 6). Transcript levels were determined by qPCR.

Data are represented as mean ± SD, n = 3 or 6, p*<0.05, **<0.01, ***<0.001, and ****<0.0001 (Student's t test). See also Star methods for details on statistical analyses performed using *R*. See also Figures S1–S3, and Tables S1–S3. H and hpi, hours post incubation.

sequenced (poly(A) enriched RNA) at 0, 1, 2, 3, 6, and 12-h post incubation (hpi). SARS-CoV-2 genome, subgenomic RNA, and transcripts were detected in infected samples; viral transcript expression clustered based on post-incubation time using principal component analysis (PCA) (see Figure S1A). In our RNA-seq analysis, we detected high levels of expression of SARS-CoV-2 structural and accessory genes at the 3′ end of the genome as early as 0 hpi (Figure 1A). Significant expression of *ORF1ab*, relative to 0 hpi was detected at 6 hpi (Figure 1B). SARS-CoV-2 nucleocapsid (*N*) gene was highly expressed relative to other genes as early as 0 hpi (Figure 1B), with relative expression significantly increasing over time ($p = 1.4 \times 10^{-16}$; Figure 1B). The absolute expression of other genes increased over time with levels of *N* > *M* > *ORF10* > *S* > *ORF1ab* > *ORF7a* > *ORF8* > *ORF3a* > *ORF6* > *E* > *ORF7b* > *ORF1a* at 12 hpi (Figure 1B and Table S1).

To determine SARS-CoV-2-infection-mediated host responses, we extracted total cellular RNA at different times post infection and analyzed gene expression in infected and mock-infected Calu-3 cells using RNA-seq. Gene expression levels in these cells clustered based on time points via PCA (see Figure S1B). One hundred twenty-four genes were significantly differentially expressed in infected cells (FDR-adjusted $p < 0.05$), relative to mock-infected cells in at least one time point post infection ($|\log_2 FC| > 1$), including genes involved in type I IFN production and signaling (Figure 1C; see Table S2 and Figures S1C and S1E). The extent of antiviral gene expression at 12 hpi correlated with an increase in viral transcripts (see Figure S1C). Interestingly, at early time points of 2 and 3 hpi, pathway enrichment analysis revealed numerous cellular processes that were significantly downregulated in SARS-CoV-2-infected cells, relative to mock-infected cells (FDR-adjusted $p < 0.05$). Downregulated processes included RNA splicing, apoptosis, ATP synthesis, and host translation, whereas genes associated with viral processes, cell adhesion, and double-stranded RNA binding were upregulated in infected cells relative to mock-infected cells at 2 and 3 hpi (Figure 1D; see Figures S1D and S2, and Table S3). Cellular pathways associated with type I IFN production and signaling, along with OAS/TRAF-mediated antiviral responses, were significantly upregulated at 12 hpi (Figures 1D and S2). Consistent with other reports (Blanco-Melo et al., 2020), transcript levels for *IFNβ1* and *IFNλ1* were significantly upregulated at 12 hpi with SARS-CoV-2 (Figure 1E). Transcript levels of *IFNλ2* and *IFNλ3* were elevated at 6 and 12 hpi, but the levels did not reach significance relative to mock-infected cells at these time points (Figure 1E).

IFN production alone is not sufficient to protect cells from invading viruses. IFNs function through ISG expression, which in turn confers antiviral protection in infected (autocrine mode of action) and neighboring (paracrine mode of action) cells (Schoggins, 2019; Schoggins and Rice, 2011). Nineteen antiviral ISGs were upregulated in infected cells, relative to mock-infected cells at 12 hpi, including interferon-induced protein with tetratricopeptide repeats 1 (*IFIT1*), interferon regulatory factor 7 (*IRF7*), 2′-5-oligoadenylate synthetase 2 (*OAS2*), and MX dynamin GTPase 1 (*MX1*) (Figure 1F; see Figure S3A and Table S2).

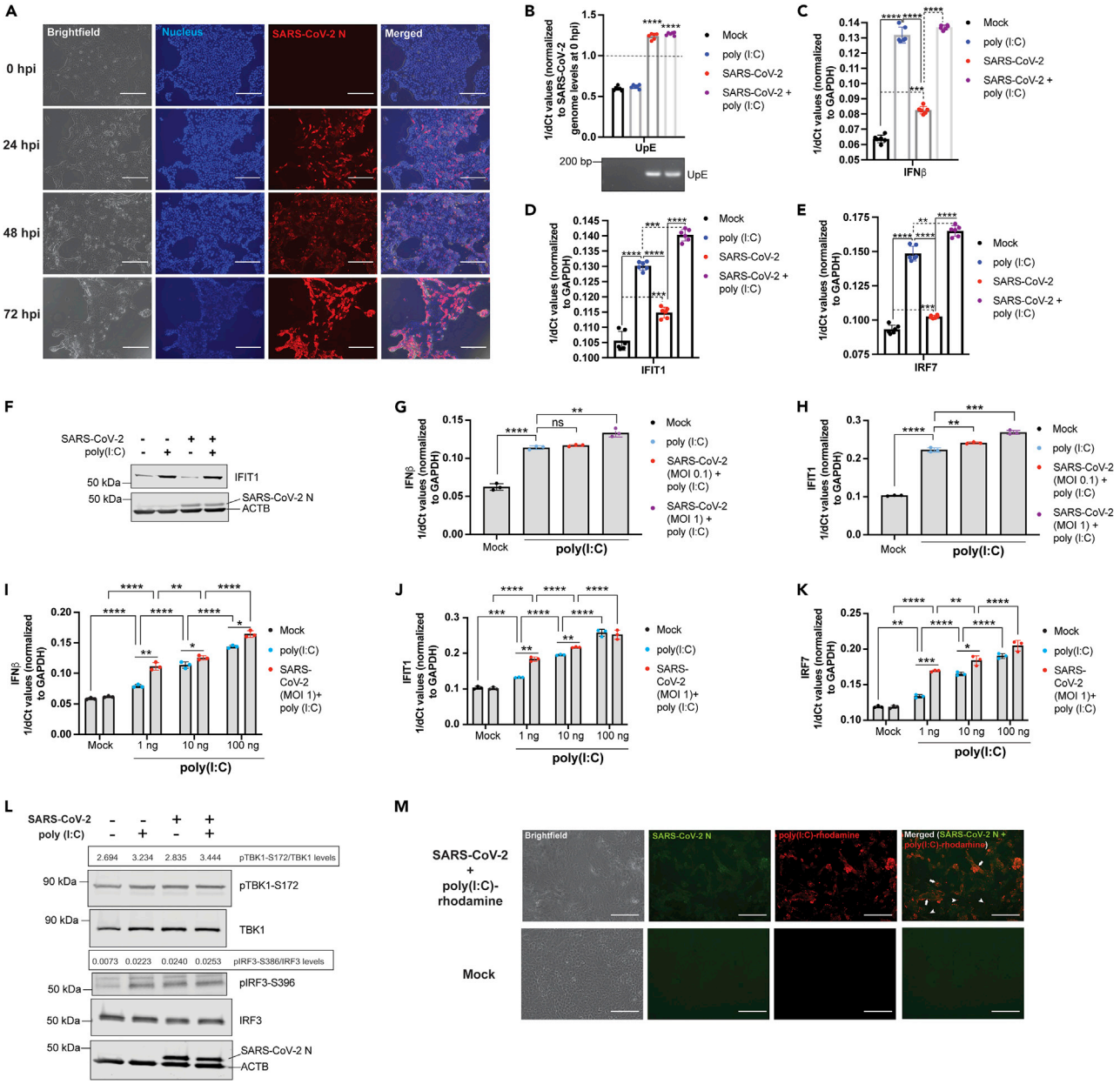

Figure 2. SARS-CoV-2 infection does not inhibit type I IFN expression

To determine if SARS-CoV-2 can modulate *IFNβ* gene expression and downstream stimulation of ISGs, Calu-3 cells were infected with SARS-CoV-2 for varying times, following which cells were mock transfected or transfected with poly(I:C). Mock-infected and mock-transfected cells served as controls. Transcript levels were quantified using qPCR. Protein expression was observed and quantified using immunoblot analysis.

(A) Calu-3 cells were infected with SARS-CoV-2 (MOI 1) for 0, 24, 48, and 72 h. Cells were fixed and stained to visualize the nucleus and SARS-CoV-2 nucleocapsid (N) protein. Scale bar indicates 300 μm.

(B) SARS-CoV-2 genome (UpE) levels in Calu-3 cells infected with SARS-CoV-2 (MOI 1) or mock infected for 12 h and transfected with 100 ng of poly(I:C) or mock transfected for 6 h (n = 6). Primers for the UpE region were designed to quantify SARS-CoV-2 genome levels (see methods). 1/dCT values are represented after normalizing Ct values for SARS-CoV-2 genome levels at 18 hpi with Ct values observed at 0 hpi (immediately after removal of virus inoculum). Gel (below): UpE qPCR amplicons were visualized on an agarose gel.

(C) *IFNβ* transcript levels in Calu-3 cells that were infected with SARS-CoV-2 (MOI 1) or mock infected for 12 h. Twelve hpi, cells were either transfected with 100 ng of poly(I:C) or mock transfected for 6 h. *IFNβ* transcript levels were normalized to *GAPDH* transcript levels (n = 6).

(D) *IFIT1* transcript levels in Calu-3 cells that were infected with SARS-CoV-2 (MOI 1) or mock infected for 12 h. Twelve hpi, cells were either transfected with 100 ng of poly(I:C) or mock transfected for 6 h. *IFIT1* transcript levels were normalized to *GAPDH* transcript levels (n = 6).

Figure 2. *Continued*

(E) *IRF7* transcript levels in Calu-3 cells that were infected with SARS-CoV-2 (MOI 1) or mock infected for 12 h. Twelve hpi, cells were either transfected with 100 ng of poly(I:C) or mock transfected for 6 h. *IRF7* transcript levels were normalized to *GAPDH* transcript levels (n = 6).

(F) IFIT1, SARS-CoV-2 N, and ACTB protein expression in Calu-3 cells that were infected with SARS-CoV-2 (MOI 1) or mock infected for 24 h. Twenty-four hpi, cells were either transfected with 1,000 ng of poly(I:C) or mock transfected for 24 h (n = 3).

(G) *IFNβ* transcript levels in Calu-3 cells that were infected with SARS-CoV-2 (MOI 0.1 or 1) or mock infected for 24 h. Twenty-four hpi, cells were transfected with 10 ng of poly(I:C) or mock transfected for 12 h. *IFNβ* transcript levels were normalized to *GAPDH* transcript levels (n = 3).

(H) *IFIT1* transcript levels in Calu-3 cells that were infected with SARS-CoV-2 (MOI 0.1 or 1) or mock infected for 24 h. Twenty-four hpi, cells were transfected with 10 ng of poly(I:C) or mock transfected for 12 h. *IFIT1* transcript levels were normalized to *GAPDH* transcript levels (n = 3).

(I) *IFNβ* transcript levels in Calu-3 cells that were infected with SARS-CoV-2 (MOI 1) or mock infected for 24 h. Twenty-four hpi, cells were either transfected with varying concentrations of poly(I:C) or mock transfected for 12 h. *IFNβ* transcript levels were normalized to *GAPDH* transcript levels (n = 3).

(J) *IFIT1* transcript levels in Calu-3 cells that were infected with SARS-CoV-2 (MOI 1) or mock infected for 24 h. Twenty-four hpi, cells were either transfected with varying concentrations of poly(I:C) or mock transfected for 12 h. *IFIT1* transcript levels were normalized to *GAPDH* transcript levels (n = 3).

(K) *IRF7* transcript levels in Calu-3 cells that were infected with SARS-CoV-2 (MOI 1) or mock infected for 24 h. Twenty-four hpi, cells were either transfected with varying concentrations of poly(I:C) or mock transfected for 12 h. *IRF7* transcript levels were normalized to *GAPDH* transcript levels (n = 3).

(L) pTBK1-S172, TBK1, pIRF3-S396, IRF3, SARS-CoV-2 N, and ACTB protein expression in Calu-3 cells that were infected with SARS-CoV-2 (MOI 1) or mock infected for 24 h. Twenty-four hpi, cells were either transfected with 1,000 ng of poly(I:C) or mock transfected for an additional 24 h (n = 3).

(M) Calu-3 cells were infected with SARS-CoV-2 (MOI 1) or mock infected for 24 h, followed by transfection with 1,000 ng of rhodamine-labeled poly(I:C) or mock transfection for 3 h. Cells were fixed and stained to visualize SARS-CoV-2 nucleocapsid (N) protein and rhodamine-labeled poly(I:C). SARS-CoV-2 N and poly(I:C)-rhodamine containing cells are indicated by arrows. Cells that only contained detectable levels of poly(I:C)-rhodamine are indicated by arrow heads. Scale bar indicates 150 μm.

Data are represented as mean ± SD, n = 3 or 6, p**<0.01, ***<0.001, and ****<0.0001 (Student's t test and Tukey's multiple comparisons test). pTBK1-S172 and pIRF3-S396 protein expression levels are expressed as ratios of pTBK1-S172/TBK1 and pIRF3-S396/IRF3 levels, respectively. Blots were quantified using Image Studio (Li-COR) (n = 3). Ct, cycle threshold. See also Figure S3.

Genes associated with structural molecule activity, cell adhesion, and exocytosis were downregulated in SARS-CoV-2-infected cells, relative to uninfected cells at 12 hpi (see Figure S2).

Coronaviruses, such as those that cause SARS and MERS, have evolved multiple proteins that can inhibit type I IFN expression (Chen et al., 2014; Lu et al., 2011; Lui et al., 2016; Niemeyer et al., 2013; Siu et al., 2014; Yang et al., 2013). To confirm our RNA-seq observations that SARS-CoV-2 infection alone is sufficient to induce type I IFN and ISG responses in Calu-3 cells, we infected cells with SARS-CoV-2 and assessed transcript levels of *IFNβ*, *IRF7*, and *IFIT1* by quantitative polymerase chain reaction (qPCR). *IFNβ* induction was observed at 12 hpi in SARS-CoV-2-infected cells, relative to mock-infected cells (Figure 1G). Consistent with the upregulation of *IFNβ* transcripts in SARS-CoV-2-infected cells, transcript levels for ISGs, such as *IRF7* and *IFIT1*, were also significantly upregulated at 12 hpi relative to mock-infected cells (Figures 1H and 1I).

SARS-CoV-2 is not adept at inhibiting exogenous stimulation of type I IFN expression

To determine if SARS-CoV-2 is able to inhibit type I IFN responses mounted against an exogenous stimulus, we infected Calu-3 cells with SARS-CoV-2 for 12 h at an MOI of 1 and stimulated these cells with exogenous double-stranded RNA [poly(I:C)] for 6 h. We confirmed SARS-CoV-2 replication in Calu-3 cells over 0, 24, 48, and 72 h of infection by staining for the nucleocapsid (N) protein (Figure 2A). We quantified SARS-CoV-2 replication by qPCR using primers designed to amplify genomic RNA by targeting a region between *ORF3a* and *E* genes. We called this region "upstream of E" (UpE). SARS-CoV-2 UpE levels were higher in SARS-CoV-2-infected cells and in SARS-CoV-2-infected + poly(I:C)-treated cells, relative to UpE levels at 0 hpi immediately after removing the inoculum (Figure 2B). We also measured the levels of *IFNβ* transcripts in these cells by qPCR. Poly(I:C) transfection alone induced higher levels of *IFNβ* transcripts relative to mock-transfected cells (Figure 2C). SARS-CoV-2 infection alone also induced higher levels of *IFNβ* transcripts relative to mock-infected cells (Figure 2C). Interestingly, there was no significant difference in *IFNβ* transcript levels between poly(I:C)-transfected and SARS-CoV-2-infected + poly(I:C)-transfected cells (Figure 2C).

To determine if *IFNβ* expression in SARS-CoV-2-infected and/or poly(I:C)-transfected cells is associated with ISG expression, we additionally quantified the levels of *IFIT1* and *IRF7*. Poly(I:C) transfection alone induced significantly higher levels of *IFIT1* and *IRF7* transcripts relative to mock-transfected cells (Figures 2D and 2E). SARS-CoV-2 infection alone also induced higher levels of *IFIT1* and *IRF7* transcripts relative to mock-infected cells (Figures 2D and 2E). Notably, *IFIT1* and *IRF7* transcript levels in SARS-CoV-2-infected + poly(I:C)-transfected cells were higher than levels in cells that were transfected with poly(I:C) alone (Figures 2D and 2E), suggesting an additive effect of SARS-CoV-2 infection on poly(I:C)-mediated gene expression.

To validate our gene expression observations, we examined SARS-CoV-2 N, IFIT1, and beta-actin (ACTB) protein expression. Poly(I:C) transfection induced higher levels of IFIT1 in Calu-3 cells, whereas SARS-CoV-2 infection did not induce higher observable levels of IFIT1 by immunoblot analysis at 48 hpi, relative to mock-infected cells (Figure 2F); however, at 72 hpi, SARS-CoV-2 infection induced higher observable levels of IFIT1 protein expression relative to mock-infected cells (see Figure S4). We confirmed SARS-CoV-2 infection in these cells by detecting N protein in the samples (Figure 2F).

To determine if the MOI of SARS-CoV-2 would influence its ability to modulate exogenous stimulation of interferon responses, we infected Calu-3 cells with two different MOIs of 0.1 and 1 for 24 h, followed by exogenous stimulation of cells with 10 ng of poly(I:C) for 12 h. Both MOIs of SARS-CoV-2 were unable to suppress the expression of *IFNβ* and *IFIT1* in poly(I:C)-stimulated cells (Figures 2G and 2H). Furthermore, a high MOI of 1 had an additive effect on the expression levels of *IFNβ* and *IFIT1* in poly(I:C)-stimulated cells (Figures 2G and 2H). Next, to determine if high concentrations of poly(I:C) in Figures 2C–2E may have overwhelmed the ability of SARS-CoV-2 to suppress IFN responses, we infected Calu-3 cells with SARS-CoV-2 for 24 h, followed by stimulation with a range of concentrations of poly(I:C) for 12 h (Figures 2I–2K). Even at the lowest poly(I:C) concentration of 1 ng, SARS-CoV-2 was unable to suppress *IFNβ*, *IFIT1*, and *IRF7* gene expression. Indeed, SARS-CoV-2 infection displayed an additive effect on the expression levels of *IFNβ* at all concentrations of poly(I:C), whereas the additive effect of SARS-CoV-2 infection on *IFIT1* and *IRF7* expression levels reached significance at concentrations of 1 ng and 10 ng of poly(I:C) (Figures 2I–2K).

Type I IFN production is primarily mediated by the phosphorylation and activation of TBK1, which in turn phosphorylates and activates IRF3 (Janeway and Medzhitov, 2002; Kawai and Akira, 2006). Activation of TBK1 is associated with phosphorylation of serine 172 (Larabi et al., 2013), whereas activation of IRF3 involves phosphorylation of serine 396, among other residues (Chen et al., 2008). To determine SARS-CoV-2 infection-induced phosphorylation of TBK1 and IRF3, we infected Calu-3 cells for 24 h followed by poly(I:C) or mock stimulation for another 24 h and performed immunoblot analysis to detect levels of TBK1 (pTBK1-S172) and IRF3 (pIRF3-S396) phosphorylation. Only modest increases in phosphorylation of TBK1 were observed in SARS-CoV-2-infected and poly(I:C)-treated cells relative to untreated cells at the time of sampling (Figure 2L). Phosphorylation of IRF3 was observed in both SARS-CoV-2-infected and poly(I:C)-treated cells relative to untreated cells, with similar levels of pIRF3-S396 observed following all infection and treatment conditions (Figure 2L).

Titrating different concentrations of poly(I:C) in Figures 2I–2K demonstrated that SARS-CoV-2 infection has an additive effect on poly(I:C)-mediated upregulation of IFN responses. In addition, we also determined if poly(I:C) was delivered to infected cells (Figure 2M). We infected Calu-3 cells with SARS-CoV-2 for 24 h, followed by transfection with rhodamine-labeled poly(I:C) for 3 h. At 24 h post infection, we could detect visible levels of SARS-CoV-2 N and poly(I:C) in Calu-3 cells (Figure 2M; arrows). Few uninfected cells (Figure 2M; arrow heads) also contained detectable levels of poly(I:C); however, as identified in Figures 2I–2K, these cells are not sufficient to mount an overwhelming IFN response, because SARS-CoV-2 infection had an additive effect on IFN and ISG expression in poly(I:C)-treated cells.

SARS-CoV-2 infection is unable to suppress downstream type I IFN signaling

SARS-CoV and MERS-CoV proteins can also inhibit downstream IFN signaling to restrict the production of ISGs (de Wit et al., 2016). To evaluate if SARS-CoV-2 can inhibit type I IFN signaling in response to exogenous IFNβ treatment, we infected Calu-3 cells for 12 h at an MOI of 1 and stimulated these cells with recombinant human IFNβ for 6 h. We monitored gene expression levels of *IRF7* and *IFIT1* in these cells by qPCR. Validation of the antiviral efficacy of our recombinant IFNβ1 was carried out in human fibroblast (THF) cells that were pretreated with IFNβ1, followed by RNA and DNA virus infections. Pre-treatment of THF cells with recombinant IFNβ1 inhibited the replication of herpes simplex virus (HSV), vesicular stomatitis virus (VSV), and H1N1 in a dose-dependent manner (see Figure S3B).

SARS-CoV-2 genome levels were significantly higher in infected cells relative to mock-infected cells (Figure 3A). Although SARS-CoV-2 UpE levels displayed a lower trend in SARS-CoV-2-infected + IFNβ-treated cells relative to SARS-CoV-2-infected-only cells, UpE levels were not significantly different after 6 h of IFNβ treatment (Figure 3A). Exogenous IFNβ treatment significantly upregulated transcript levels of *IRF7* and *IFIT1* relative to mock-treated Calu-3 cells (Figures 3B and 3C). Consistent with our RNA-seq data, SARS-CoV-2 infection induced mild but significant levels of *IRF7* and *IFIT1* transcripts relative to

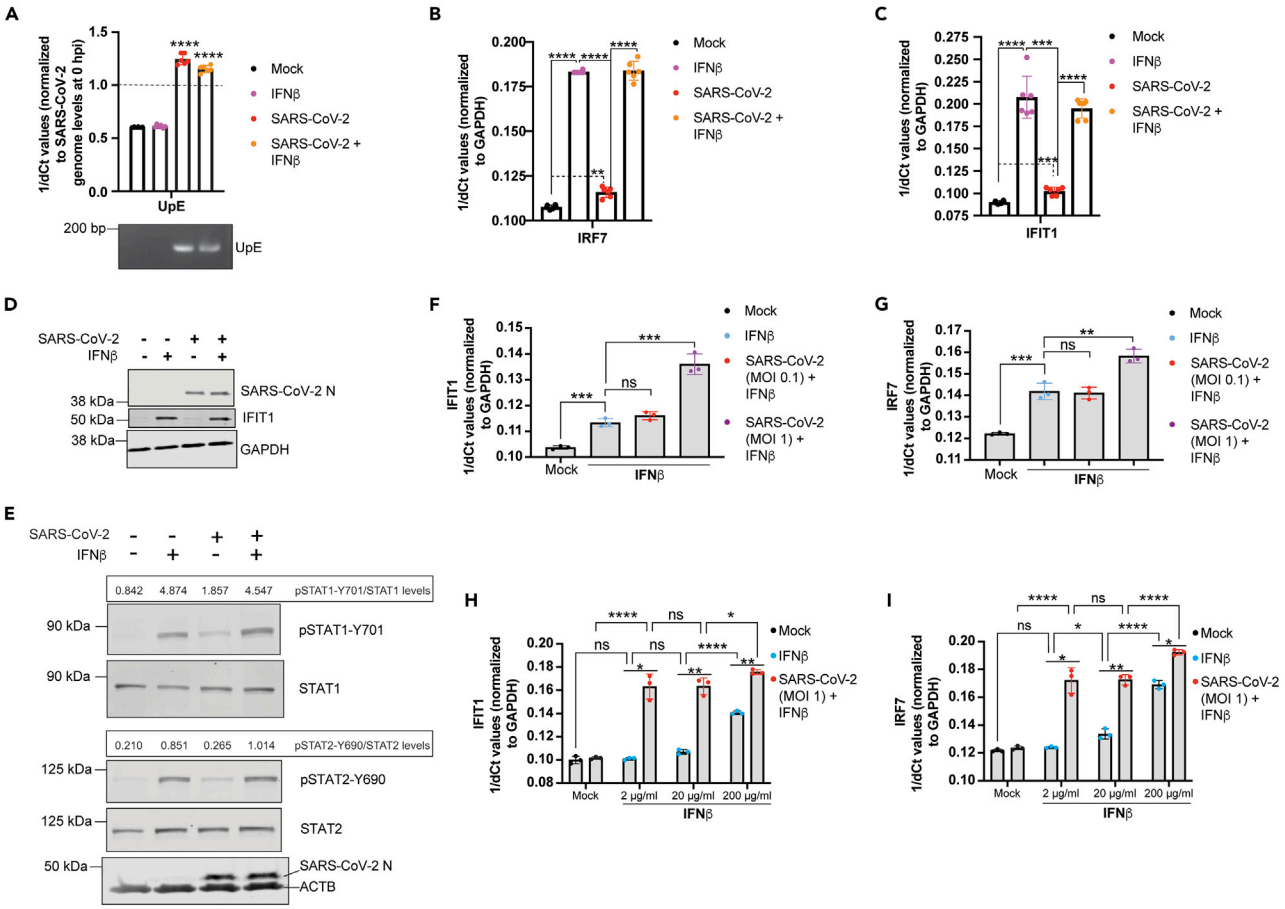

Figure 3. SARS-CoV-2 is unable to inhibit type I IFN signaling

To determine if SARS-CoV-2 can inhibit IFNβ-mediated stimulation of ISGs, such as IFIT1, Calu-3 cells were infected with SARS-CoV-2 for 12 or 24 h, following which cells were mock treated or treated with recombinant IFNβ. Mock-infected and mock-treated cells served as controls. Transcript levels were quantified using qPCR, and protein expression was observed using immunoblots.

(A) SARS-CoV-2 genome (UpE) levels in Calu-3 cells infected with SARS-CoV-2 (MOI 1) or mock infected for 12 h and treated with recombinant IFNβ or mock treated for 6 h (n = 6). 1/dCT values are represented after normalizing Ct values for SARS-CoV-2 genome levels at 18 hpi with Ct values observed at 0 hpi (immediately after removal of virus inoculum). Gel (below): UpE qPCR amplicons were visualized on an agarose gel.

(B) *IRF7* transcript levels in Calu-3 cells that were infected with SARS-CoV-2 (MOI 1) or mock infected for 12 h. Twelve hpi, cells were either treated with recombinant IFNβ or mock treated for 6 h. *IRF7* transcript levels were normalized to *GAPDH* transcript levels (n = 6).

(C) *IFIT1* transcript levels in Calu-3 cells that were infected with SARS-CoV-2 (MOI 1) or mock infected for 12 h. Twelve hpi, cells were either treated with recombinant IFNβ or mock treated for 6 h. *IFIT1* transcript levels were normalized to *GAPDH* transcript levels (n = 6).

(D) SARS-CoV-2 N, IFIT1, and GAPDH protein expression in Calu-3 cells that were infected with SARS-CoV-2 (MOI 1) or mock infected for 12 h. Twelve hpi, cells were either treated with recombinant IFNβ or mock treated for 6 h (n = 3).

(E) pSTAT1-Y701, STAT1, pSTAT2-Y690, STAT2, SARS-CoV-2 N, and ACTB protein expression in Calu-3 cells that were infected with SARS-CoV-2 (MOI 1) or mock infected for 24 h. Twenty-four hpi, cells were either treated with recombinant IFNβ or mock treated for 30 min (n = 3).

(F) *IFIT1* transcript levels in Calu-3 cells that were infected with SARS-CoV-2 (MOI 0.1 or 1) or mock infected for 24 h. Twenty-four hpi, cells were mock treated or treated with recombinant IFNβ containing media (20 μg/mL total protein) for 12 h. *IFIT1* transcript levels were normalized to *GAPDH* transcript levels (n = 3).

(G) *IRF7* transcript levels in Calu-3 cells that were infected with SARS-CoV-2 (MOI 0.1 or 1) or mock infected for 24 h. Twenty-four hpi, cells were mock treated or treated with recombinant IFNβ-containing media (20 μg/mL total protein) for 12 h. *IRF7* transcript levels were normalized to *GAPDH* transcript levels (n = 3).

(H) *IFIT1* transcript levels in Calu-3 cells that were infected with SARS-CoV-2 (MOI 1) or mock infected for 24 h. Twenty-four hpi, cells were either treated with varying concentrations of recombinant IFNβ or mock treated for 12 h. *IFIT1* transcript levels were normalized to *GAPDH* transcript levels (n = 3).

(I) *IRF7* transcript levels in Calu-3 cells that were infected with SARS-CoV-2 (MOI 1) or mock infected for 24 h. Twenty-four hpi, cells were either treated with varying concentrations of recombinant IFNβ or mock treated for 12 h. *IRF7* transcript levels were normalized to *GAPDH* transcript levels (n = 3).

Data are represented as mean ± SD, n = 3 or 6, ns: not significant, p*<0.05, p**<0.01, ***<0.001, and ****<0.0001 (Student's t test and Tukey's multiple comparison's test). Ct, cycle threshold. pSTAT1-Y701 and pSTAT2-Y690 protein expression levels are expressed as ratios of pSTAT1-Y701/STAT1 and pSTAT2-Y690/STAT2 levels, respectively. Blots were quantified using Image Studio (Li-COR) (n = 3). For IFNβ treatment, cell culture supernatant containing recombinant IFNβ was used. Cell culture supernatant containing 2 mg/mL of total protein, including IFNβ, was used in A-E. A range of concentrations was used for other figures as indicated. Ct, cycle threshold. See Star methods for recombinant IFNβ generation. See also Figures S3 and S4.

mock-infected cells (Figures 3B and 3C). IFNβ-mediated induction of *IRF7* and *IFIT1* was not dampened by SARS-CoV-2 infection (Figures 3B and 3C).

To validate our transcriptional responses, we repeated our experiments with exogenous IFNβ treatment and determined if SARS-CoV-2 could inhibit type I IFN-mediated upregulation of IFIT1 at the protein level. SARS-CoV-2 infection alone failed to induce detectable levels of IFIT1 at 12 hpi (Figure 3D). IFNβ treatment with or without prior 12 h of SARS-CoV-2 infection induced robust expression of IFIT1 (Figure 3D). We confirmed SARS-CoV-2 infection in these cells by immunoblotting for N protein (Figure 3D).

Binding of IFNs to their receptors activates a series of downstream signaling events, which involves phosphorylation of STAT1 at tyrosine 701 (pSTAT1-Y701) and STAT2 at tyrosine 690 (pSTAT2-Y690) (Pilz et al., 2003; Steen and Gamero, 2013). To determine if SARS-CoV-2 can inhibit phosphorylation of STAT1 and STAT2 proteins, we infected Calu-3 cells with SARS-CoV-2 for 24 h followed by 30 min of stimulation with or without recombinant IFNβ. SARS-CoV-2 infection alone induced mild pSTAT1-Y701 and pSTAT2-Y690 levels relative to mock-infected cells, albeit lower than levels observed in exogenous IFNβ-treated cells (Figure 3E). Importantly, SARS-CoV-2 infection was unable to inhibit pSTAT1-Y701 and pSTAT2-Y690 levels in cells treated with IFNβ (Figure 3E).

To determine if the MOI of SARS-CoV-2 would influence its ability to suppress exogenous stimulation of interferon responses, we infected Calu-3 cells with two different MOIs of 0.1 and 1 for 24 h, followed by exogenous stimulation of cells with IFNβ for 12 h. Infection with both MOIs of SARS-CoV-2 was unable to suppress the expression of *IFIT1* and *IRF7* on IFNβ treatment (Figures 3F and 3G). Furthermore, high MOI 1 of SARS-CoV-2 had an additive effect on the expression of *IFIT1* and *IRF7* in IFNβ-treated cells (Figures 3F and 3G). Next, to determine if high concentrations of IFNβ in Figures 3A–3D may have overwhelmed the ability of SARS-CoV-2 to suppress IFN-mediated responses, we infected Calu-3 cells with SARS-CoV-2 for 24 h, followed by stimulation with a range of concentrations of IFNβ for 12 h (Figures 3H and 3I). SARS-CoV-2 was unable to suppress *IFIT1* and *IRF7* gene expression. MOI 1 of SARS-CoV-2 had an additive effect on the expression of *IFIT1* and *IRF7* in IFNβ-treated cells at all concentrations of IFNβ (Figures 3H and 3I).

Cytokine levels in COVID-19 patients and effect of type I IFNs on SARS-CoV-2 replication

To evaluate type I IFN and other infection-associated cytokines in COVID-19 patients, we analyzed acute sera (<21 days from symptom onset) from 20 COVID-19 positive patients, of whom 10 were categorized as "moderate" cases requiring hospital admission but not admission to intensive care unit (ICU). The remaining 10 samples were from "severe" cases that required ICU admission or died. For severe cases, 6/10 patients died, and 10/10 moderate cases were discharged (see Table S4). We also included sera from five healthy, uninfected individuals. Sera from moderate cases of COVID-19 displayed significantly higher levels of platelet-derived growth factor AA (PDGF-AA) and PDGF-AB/BB relative to uninfected individuals (Figure 4). Patients with severe COVID-19 displayed higher levels of PDGF-AA, PDGF-AB/BB, GROα (CXCL-1), CXCL-9, MIP-1β, and vascular endothelial growth factor A (VEGF-A) relative to healthy individuals (Figure 4). In addition, severe cases of COVID-19 displayed an increasing trend for levels of interleukin-6 (IL-6), IL-5, macrophage colony stimulating factor 1 (M-CSF), IL-8, tumor necrosis factor alpha (TNFα), TNFβ, and granulocyte colony stimulating factor 1 (G-CSF) relative to healthy individuals and moderate cases of COVID-19. In addition, both moderate and severe cases of COVID-19 displayed an increasing trend for IL-7 and IP-10 relative to healthy controls, although the data were not significant due to wide within-patient variation in acute serum samples. Moderate cases of COVID-19 displayed an increasing trend for levels of IFN-α2 and IL-10 relative to healthy individuals and severe cases of COVID-19 (Figure 4 and see Tables S4 and S5).

To determine if exogenous IFNβ treatment can inhibit SARS-CoV-2 replication, we infected Calu-3 cells for 1 h, following which we either mock treated or treated the cells with recombinant IFNβ for 72 h. Exogenous IFNβ treatment reduced SARS-CoV-2 genome (UpE) and N protein levels in these cells (Figure 4B), consistent with an increase in IFIT1 levels (Figures 4B and S4).

Next, to determine if levels of IFN-α2 that were detected in sera from patients who developed moderate COVID-19 (Figure 4A and see Table S5) were sufficient to induce an IFN response, we tested a range of concentrations of IFN-α2 against SARS-CoV-2. Calu-3 cells contained higher levels of *IFIT1* transcripts in the presence of medium (1 ng/mL) and high (10 ng/mL) concentrations of IFN-α2, whereas *IRF7* transcript

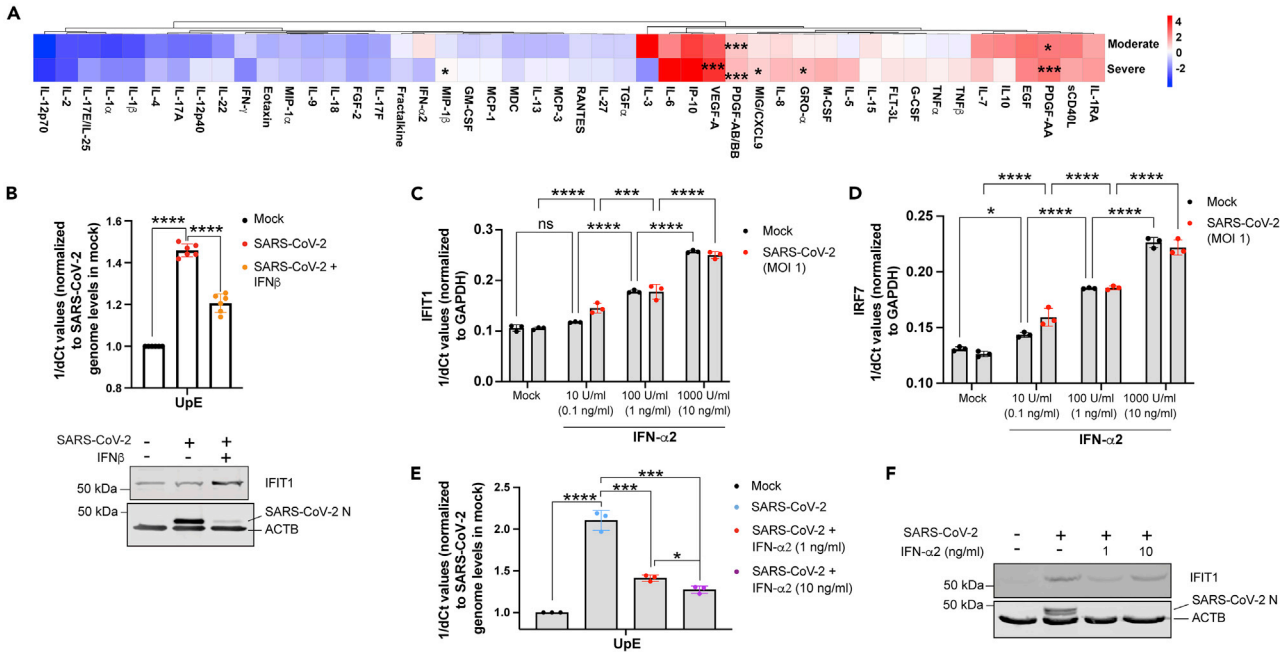

Figure 4. Cytokine protein levels in human sera from moderate and severe cases of COVID-19 relative to healthy controls and effect of type I IFNs on SARS-CoV-2 replication

(A) To determine protein levels of cytokines in sera from moderate and severe cases of COVID-19 relative to healthy controls, we analyzed protein levels in sera using a 48-plex human cytokine and chemokine array. Mean $\log_2$ fold-change in serum cytokine protein levels in patients with moderate (n = 10) or severe (n = 10) case of COVID-19, relative to levels in healthy donors (n = 5) are represented here.

(B) SARS-CoV-2 genome (UpE) levels in Calu-3 cells infected with SARS-CoV-2 (MOI 1) or mock infected for 1 h followed by treatment with recombinant IFNβ or mock treatment for 72 h (n = 6). 1/dCT values are represented after normalizing Ct values for SARS-CoV-2 genome levels in infected cells (with or without recombinant IFNβ treatment) with Ct values observed in mock-infected cells. Blot (below): IFIT1, SARS-CoV-2 N, and ACTB protein expression in Calu-3 cells that were infected with SARS-CoV-2 or mock infected for 1 h, followed by treatment with recombinant IFNβ or mock treatment for 72 h (n = 3). For IFNβ treatment, cell culture supernatant containing 2 mg/mL of total protein, including IFNβ was used.

(C) *IFIT1* transcript levels in Calu-3 cells that were infected with SARS-CoV-2 (MOI 1) or mock infected for 24 h. Twenty-four hpi, cells were treated with varying concentrations of recombinant IFN-α2 or mock treated for 6 h. *IFIT1* transcript levels were normalized to *GAPDH* transcript levels (n = 3).

(D) *IRF7* transcript levels in Calu-3 cells that were infected with SARS-CoV-2 (MOI 1) or mock infected for 24 h. Twenty-four hpi, cells were treated with varying concentrations of recombinant IFN-α2 or mock treated for 6 h. *IRF7* transcript levels were normalized to *GAPDH* transcript levels (n = 3).

(E) SARS-CoV-2 genome (UpE) levels in Calu-3 cells infected with SARS-CoV-2 (MOI 1) or mock infected for 1 h followed by treatment with recombinant IFN-α2 (1 ng/mL or 10 ng/mL) or mock treatment for 72 h (n = 3). 1/dCT values are represented after normalizing Ct values for SARS-CoV-2 genome levels in infected cells (with or without recombinant IFN-α2 treatment) with Ct values observed in mock-infected cells.

(F) IFIT1, SARS-CoV-2 N, and ACTB protein expression in Calu-3 cells that were infected with SARS-CoV-2 (MOI 1) or mock infected for 1 h, followed by treatment with recombinant IFN-α2 (1 ng/mL or 10 ng/mL) or mock treatment for 72 h (n = 3).

Data are represented as mean ± SD, n = 5 for healthy human controls, and n = 10 each for moderate or severe cases of COVID-19, n = 3 or 6 for *in vitro* experiments. p*<0.05, p**<0.01, p***<0.001, and p****<0.0001 (Student's t tests with Benjamini-Hochberg multiple testing correction, Student's t tests and Tukey's multiple comparison test). See also Tables S4 and S5, and Figure S3.

levels were higher in Calu-3 cells treated with low (0.1 ng/mL), medium, or high concentrations of IFN-α2 (Figures 4C and 4D). Furthermore, consistent with our data for IFNβ, SARS-CoV-2 infection was unable to suppress IFN-α2-mediated expression of ISGs, such as *IFIT1* and *IRF7* (Figures 4C and 4D). Finally, to determine if IFN-α2 was capable of suppressing SARS-CoV-2 replication, we infected Calu-3 cells with SARS-CoV-2 and treated the cells with two concentrations of IFN-α2 (1 ng/mL and 10 ng/mL) for 72 h. Both concentrations of IFN-α2 significantly reduced SARS-CoV-2 replication (Figures 4E and 4F).

DISCUSSION

SARS-CoV-2 emerged in December 2019 to cause a global pandemic of COVID-19 (Dong et al., 2020; Zhou et al., 2020a). Clinical observations and emerging data from *in vitro* and *in vivo* studies have demonstrated the ability of SARS-CoV-2 to induce type I IFNs (Blanco-Melo et al., 2020; Rebendenne et al., 2021; Yin et al., 2021). However, a recent review summarized studies that suggest that antiviral IFN responses are dampened in COVID-19 patients (Acharya et al., 2020). Emerging data also suggest that timing and extent of

interferon production is likely associated with manifestation of disease severity (Zhou et al., 2020b). In spite of some progress in understanding how SARS-CoV-2 activates antiviral responses, mechanistic studies into SARS-CoV-2-infection-mediated induction and modulation of human type I IFN responses are lacking. To understand SARS-CoV-2-infection-induced pathogenesis during the clinical course of COVID-19, it is imperative that we understand if and how replicating SARS-CoV-2 interacts with type I IFN responses. These observations can be leveraged to develop drug candidates and inform ongoing drug trials, including trials that involve type I and III IFNs.

In this study, a time-series RNA-seq analysis of poly(A))-enriched RNA from SARS-CoV-2-infected human airway epithelial cells allowed us to map the progression of SARS-CoV-2 replication and transcription. As observed with other coronaviruses (Fehr and Perlman, 2015; Lai, 1990; Perlman and Netland, 2009), SARS-CoV-2 replicated and transcribed sub-genomic RNA and mRNA in a directional manner (Figures 1A and 1B). Thus, our data demonstrate that SARS-CoV-2 replication strategy is consistent with other coronaviruses. Furthermore, our data demonstrate that Calu-3 cells support SARS-CoV-2 replication and that these cells represent a good *in vitro* model to study SARS-CoV-2-host interactions, as reported by others (Blanco-Melo et al., 2020; Yin et al., 2021).

Studies have demonstrated that ectopically expressed SARS-CoV-2 proteins can suppress type I IFN responses. Low SARS-CoV-2-induced type I IFN responses may be associated with (1) the virus' ability to mask the detection of viral RNA by cellular PRRs and/or (2) the ability of viral proteins to inactivate cellular mechanisms involved in type I IFN induction (Shin et al., 2020). Data from our studies show that infection with wild-type and replication competent SARS-CoV-2 is capable of inducing a type I IFN response in human airway epithelial cells, including upregulation of IFN expression (Figures 1C, 1E and 1G) and downstream IFN signaling genes (Figures 1C, 1F, 1H, 1I and S4). Our observations corroborate and expand upon recent data from Lei, Rebendenne, and Yin et al.'s studies where the authors have demonstrated that SARS-CoV-2 infection is capable of upregulating type I IFN responses in multiple human cell types (Lei et al., 2020; Rebendenne et al., 2021; Yin et al., 2021).

The physiological relevance of an existing but dampened type I IFN response to SARS-CoV-2 remains to be identified. Emerging data suggest that prolonged and high levels of type I IFNs correlate with COVID-19 disease severity (Lucas et al., 2020). Thus, a dampened yet protective early type I IFN response against SARS-CoV-2 may in fact be beneficial for humans (Park and Iwasaki, 2020). However, questions remain about how a low-type I IFN response against SARS-CoV-2 could play a protective role during infection. One possibility is that low levels of type I IFN production is sufficient to control SARS-CoV-2 replication (Figure 4E). This may explain the large number of asymptomatic cases of SARS-CoV-2 where an early IFN response may control virus replication and disease progression. Indeed, in one study, type I IFN (IFNα) levels were higher in asymptomatic cases relative to symptomatic cases (n = 37) (Long et al., 2020). Further studies are required to identify regulatory mechanisms behind the protective role of a controlled and early IFN response during SARS-CoV-2 infection versus the delayed and potentially damaging long-term IFN response observed in some severe cases of COVID-19.

In one study, SARS-CoV was demonstrated to inhibit poly(I:C)-mediated upregulation of IFNβ (Lu et al., 2011). Our data show that infection with SARS-CoV-2 is unable to inhibit poly(I:C)-mediated upregulation of *IFNβ* transcripts and downstream ISGs, such as *IFIT1* and *IRF7* (Figures 2C–2E). Indeed, SARS-CoV-2 infection, followed by poly(I:C) transfection induced higher levels of *IFNβ* and ISG (*IFIT1* and *IRF7*) transcripts relative to poly(I:C) alone, indicating that wild-type infection partially augments poly(I:C)-mediated upregulation of type I IFN signaling (Figures 2C–2E and 2G–2K) in Calu-3 cells. Furthermore, low or high MOI of SARS-CoV-2 was unable to suppress IFN responses stimulated by poly(I:C) (Figures 2G and 2H). A high MOI of SARS-CoV-2 was also unable to suppress IFN responses stimulated by a range of poly(I:C) concentrations (Figures 2I–2K). Thus, it is important to identify the kinetics and landscape of virus infection, transcription and translation, and how that may regulate human type I IFN responses. Although multiple studies have demonstrated that ectopically expressed SARS-CoV-2 proteins can suppress type I IFN responses, there is a need to study the dynamic interplay between viral RNA-mediated induction of IFN responses, followed by subsequent dampening of these responses, as viral proteins accumulate in infected cells. It is also important to identify SARS-CoV-2-host interactions in different human cell types to discern cell-type-specific differences in IFN responses. Furthermore, as multiple SARS-CoV-2 variants continue to evolve, it is important to assess the ability of these emerging variants to modulate human type I IFN responses.

Coronaviruses, including highly pathogenic SARS-CoV, MERS-CoV, and porcine epidemic diarrhea virus (PEDV) have evolved proteins that can efficiently inhibit type I IFN responses (Chen et al., 2014; Ding et al., 2014; Lu et al., 2011; Lui et al., 2016; Niemeyer et al., 2013; Siu et al., 2014; Xing et al., 2013; Yang et al., 2013). In spite of observing statistically significant upregulation of type I IFNs and ISGs at 12 hpi with SARS-CoV-2 (Figure 1), in preliminary studies we were unable to observe detectable levels of pIRF3-S396 prior to accumulation of antiviral mRNAs. We have previously shown that antiviral responses can be induced in the absence of prototypic markers of IRF3 activation such as dimerization and hyperphosphorylation, even when IRF3 was shown to be essential (Noyce et al., 2009). The simplest interpretation is that early activation of IRF3-mediated IFN responses requires low (or even undetectable) levels of pIRF3-S396, which accumulate to detectable levels over time (Figure 2L).

SARS-CoV and MERS-CoV can inhibit phosphorylation and activation of STAT1 and STAT2, which blocks global IFN-induced antiviral responses (de Wit et al., 2016). Our data demonstrate that SARS-CoV-2 infection induces phosphorylation of STAT1 and STAT2 (Figure 3E), along with upregulation of ISGs, such as *IRF7* and *IFIT1* (Figures 3B and 3C). In addition, SARS-CoV-2 infection is unable to inhibit the activation of STAT1 and STAT2 by exogenous type I IFN (Figure 3E), along with the expression of downstream ISGs, such as *IRF7* and *IFIT1* (Figures 3B and 3C and see Figure S4). Although SARS-CoV-2 infection alone induced low levels of type I IFN (Figures 1E and 2B), it was sufficient to activate STAT proteins (Figure 3E) and downstream ISG expression (Figures 2B, 2C, 3B and 3C; see Figures S1 and S3). Thus, the dampened ability of SARS-CoV-2 to inhibit downstream type I IFN responses compared with other zoonotic CoVs extends support to our hypothesis that the pathogenic consequences of a dampened type I IFN response may be largely negated by the sensitivity of SARS-CoV-2 to this response. Indeed, in our studies, exogenous type I IFN (IFNβ1 and IFN-α2) treatment significantly reduced SARS-CoV-2 replication in human airway epithelial cells (Figures 4B, 4E and 4F), consistent with a recent study that compared the susceptibility of SARS-CoV and SARS-CoV-2 to type I IFNs (Lokugamage et al., 2020). Recent studies have identified the role of an impaired type I IFN response in COVID-19 disease severity (Bastard et al., 2020; Zhang et al., 2020), which support our conclusion that SARS-CoV-2 is capable of inducing a type I IFN response, and perhaps the inability of the host to mount this response contributes to disease severity. In addition, our data provide promising support for ongoing clinical trials that include type I IFN treatment.

Studies have demonstrated that COVID-19 patients mount a dysregulated immune response, which is associated with a poor clinical outcome (Lucas et al., 2020). In our study, we observed that patients with moderate or severe case of COVID-19 had elevated serum levels of growth factors PDGF-AA and PDGF-AB/BB relative to healthy controls (Figure 4A and Tables S4 and S5). The role of PDGFs in driving disease pathology has been described previously (Andrae et al., 2008), and therapeutic use of PDGF antagonists has also been recommended (Grimminger and Schermuly, 2010; Sadiq et al., 2015). PDGF-BB has also been introduced in the clinic as a wound-healing therapy (Yamakawa and Hayashida, 2019). The physiological impact of elevated PDGF levels and cellular factors that regulate the expression of PDGF in COVID-19 patients remains to be understood.

Sera from patients with moderate case of COVID-19 contained higher levels of IL-10 relative to severe cases, which is suggestive of an anti-inflammatory response (Couper et al., 2008; Pripp and Stanisic, 2014) (Figure 4A and Tables S4 and S5). On the contrary, sera from patients with severe case of COVID-19 displayed a higher trend for levels of IL-6, IL-8, and TNFα relative to moderate cases, which is suggestive of a pro-inflammatory response (Figure 4A and Tables S4 and S5) (Lucas et al., 2020; Mandel et al., 2020; Pripp and Stanisic, 2014). Observations from our study (Figure 4A), along with other recent reports (Long et al., 2020; Lucas et al., 2020), warrant further investigations into mechanistic regulation of pro- and anti-inflammatory processes in SARS-CoV-2-infected human airway cells. Identifying regulatory proteins, such as transcription factors that contribute to a pro-inflammatory cytokine response or "cytokine storm" in SARS-CoV-2-infected individuals, will inform the selection and utilization of anti-inflammatory drugs.

Patients with moderate COVID-19 demonstrated an increasing trend for type I IFN (IFN-α2) relative to severe cases and healthy controls (Figure 4A). In a separate study, IFN-α levels were also higher in asymptomatic patients relative to symptomatic COVID-19 patients (Long et al., 2020). The presence

of type I IFN in moderate cases of COVID-19 in our study, along with a recent study by Lucas et al., suggest that SARS-CoV-2 infection is capable of inducing a type I IFN response *in vivo*; however, emerging clinical data suggest that the extent and duration of type I IFN response may dictate the clinical course of COVID-19 (Hadjadj et al., 2020b; Lucas et al., 2020). In our study, sera from COVID-19 patients were collected at admission (all <21 days post symptom onset). Early induction of IFN-α2 in moderate cases of COVID-19 may provide an antiviral advantage. Indeed, we were able to demonstrate that a range of physiologically detected concentrations of IFN-α2 was capable of inducing an antiviral response in human airway epithelial cells and that SARS-CoV-2 was unable to suppress ISG expression induced by physiologically detected concentrations of IFN-α2 (Figures 4C and 4D). Furthermore, two different concentrations of IFN-α2 (1 and 10 ng/mL) were able to reduce SARS-CoV-2 replication in human airway epithelial cells (Figure 4E). Thus, extrapolating from our *in vitro* testing of a range of IFN-α2 concentrations, we speculate that the levels of IFN-α2 detected in sera from moderate cases of COVID-19 would be sufficient to suppress SARS-CoV-2 replication. We were unable to detect IFN-α2 in severe COVID-19 patients at the time of sample collection (<21 days from first symptom onset). Thus, early upregulation of type I IFN responses such as IFN-α2 may be a predictor of moderate COVID-19 disease severity. Additional studies with later samples from severe COVID-19 patients will identify if there is a late and prolonged induction of type I IFNs as reported recently by Lucas et al. (Lucas et al., 2020). In spite of recent progress in understanding type I IFN responses in COVID-19 patients, factors associated with early or delayed and short-acting versus prolonged type I IFN induction in COVID-19 patients are poorly understood. Our *in vitro* experiments are not sufficient to capture SARS-CoV-2-IFN interactions in a model of severe COVID-19. There is a need to develop appropriate animal models to accurately represent and study the full spectrum of COVID-19 disease severities.

In conclusion, our study demonstrates that SARS-CoV-2 is a weak stimulator of type I IFN production in infected human airway epithelial cells, relative to poly(I:C). However, our data suggest that low levels of type I IFN response in SARS-CoV-2-infected cells is sufficient to activate downstream expression of antiviral ISGs. In addition, our data demonstrate that SARS-CoV-2 is unable to inhibit downstream IFN responses that are mediated by STAT proteins, which is promising for the development of type I IFNs as treatment or post-exposure prophylactics (Hoagland et al., 2021; Pereda et al., 2020). Clinical trials for combination IFNβ therapy against MERS-CoV are currently ongoing (Arabi et al., 2020). IFNβ, in combination with lopinavir-ritonavir and ribavirin, has been used with promising results in COVID-19 patients (Hung et al., 2020). Nebulized IFNβ is part of the standard of care for COVID-19 patients in China (Xu et al., 2020). Furthermore, we also demonstrate that levels of IFN-α2 detected in sera from patients with moderate COVID-19 can (A) induce an antiviral ISG response in human airway epithelial cells and (B) inhibit SARS-CoV-2 replication. Thus, our study highlights the dynamic nature of virus-host interaction during the course of SARS-CoV-2 infection and raises intriguing questions about the role and timing of IFN responses in predicting the likely severity of COVID-19.

LIMITATIONS OF THE STUDY

Although recent studies have demonstrated the ability of SARS-CoV-2 to induce IFN responses (Rebendenne et al., 2021; Yin et al., 2021), other studies have demonstrated the ability of SARS-CoV-2 proteins to suppress IFN responses (Jiang et al., 2020), along with inducing a delayed type I IFN response in SARS-CoV-2-infected cells (Lei et al., 2020). In our study, we demonstrate that SARS-CoV-2 can induce a type I IFN response in human airway epithelial cells. The human respiratory tract is made up of more than one cell type that can be infected with SARS-CoV-2, thus it is important to characterize type I IFN responses in the full range of susceptible human airway and lung cell types. In this study, we did not assess the ability of SARS-CoV-2 to mount a more potent IFN response in the absence of known IFN modulating viral proteins that have been identified in other studies. Future studies will need to assess the full potential of IFN responses in cells infected with wild-type and deletion variants of SARS-CoV-2. More work is also needed to identify the detailed kinetics of IFN induction by SARS-CoV-2 RNA in human cells, followed by subsequent modulation of IFN responses by viral proteins. This will be particularly important to understand why some patients mount a detectable IFN response, whereas others do not. Timing, intensity, and duration of type I IFN responses will be important to understand the range of disease outcomes in COVID-19 patients. Other members of *Betacoronavirus* continue to infect humans, along with infections with emerging variants of SARS-CoV-2. Thus, it is important to assess the efficacy of IFN responses against a range of human coronaviruses to determine differences in pathogenesis and disease severity.

STAR★METHODS

Detailed methods are provided in the online version of this paper and include the following:

- KEY RESOURCES TABLE
- RESOURCE AVAILABILITY
  - Lead contact
  - Materials availability
  - Data and code availability
- EXPERIMENTAL MODEL AND SUBJECT DETAILS
  - Cells and viruses
  - Subject details
- METHOD DETAILS
  - RNA-Seq
  - Cytokine levels in COVID-19 patient sera
  - Poly(I:C) transfection and IFN treatment
  - Quantitative PCR
  - Agarose gel electrophoresis
  - Immunoblots
  - Immunofluorescent microscopy
  - Antiviral bioassay
- QUANTIFICATION AND STATISTICAL ANALYSIS
  - Transcript quantification and differential expression analysis
  - Viral transcript quantification
  - Viral genome mapping
  - Cellular pathway enrichment analysis
  - Statistical analysis

SUPPLEMENTAL INFORMATION

Supplemental information can be found online at https://doi.org/10.1016/j.isci.2021.102477.

ACKNOWLEDGEMENTS

This study was supported by a Canadian Institutes of Health Research (CIHR) COVID-19 rapid response grant to principal investigator K.M. and co-investigators A.B., A.G.M., M.S.M., and S.M. A.B. was funded by the Natural Sciences and Engineering Research Council of Canada (NSERC). Computer resources were in part supplied by the McMaster Service Lab and Repository computing cluster, funded in part by grants to A.G.M. from the Canadian Foundation for Innovation. J.A.H. is supported by the Canada Research Chairs Program and an Ontario Early Career Researcher Award. M.S.M. is supported by a CIHR COVID-19 rapid response grant, a CIHR New Investigator Award, and an Ontario Early Researcher Award. ATI is supported by a Zhejiang University scientific research fund for COVID-19 prevention and control. The graphical abstract was created using BioRender.com.

AUTHOR CONTRIBUTIONS

Conceptualization, A.B., D.R., P.B., H.M., A.G.M., A.C.D., J.A.A., and K.M.; Methodology, A.B., N.E–.S., P.B., R.A.J., D.R., H.M., W.L.D., K.B., M.R.D., J.C.A., T.M., B.J.-M.T., S.A., M.K., and L.Y.; Formal analysis, A.B., N.E-.S., P.B., D.R., H.M., J.A.A, K.B., B.J.-M.T., and M.K.; Reagents, J.A.H., A.J.M, and M.S.M.; Funding acquisition, A.B., M.O., J.A.H., R.K., T.D.C., M.S.M., B.W., S.M., A.G.M, A.C.D., and K.M.; Writing—reviewing and editing A.B., N.E-.S., P.B., D.R., H.M., J.A.A., K.B., J.A.H, A.T.I, A.G.M., A.C.D., and K.M. All authors reviewed the final manuscript. Supervision, A.B., T.D.C, M.S.M., B.W., S.M., A.G.M, A.C.D., and K.M.

DECLARATION OF INTERESTS

The authors declare no competing interests.

Received: October 30, 2020
Revised: February 26, 2021
Accepted: April 23, 2021
Published: May 21, 2021

REFERENCES

Acharya, D., Liu, G., and Gack, M.U. (2020). Dysregulation of type I interferon responses in COVID-19. Nat. Rev. Immunol. *20*, 397–398.

Aguiar, J.A., Huff, R.D., Tse, W., Stampfli, M.R., McConkey, B.J., Doxey, A.C., and Hirota, J.A. (2019). Transcriptomic and barrier responses of human airway epithelial cells exposed to cannabis smoke. Physiol. Rep. *7*, e14249.

Andrae, J., Gallini, R., and Betsholtz, C. (2008). Role of platelet-derived growth factors in physiology and medicine. Genes Dev. *22*, 1276–1312.

Arabi, Y.M., Asiri, A.Y., Assiri, A.M., Aziz Jokhdar, H.A., Alothman, A., Balkhy, H.H., AlJohani, S., Al Harbi, S., Kojan, S., Al Jeraisy, M., et al. (2020). Treatment of Middle East respiratory syndrome with a combination of lopinavir/ritonavir and interferon-beta1b (MIRACLE trial): statistical analysis plan for a recursive two-stage group sequential randomized controlled trial. Trials *21*, 8.

Banerjee, A., Baid, K., and Mossman, K. (2019). Molecular pathogenesis of Middle East respiratory syndrome (MERS) coronavirus. Curr. Clin. Microbiol. Rep. *6*, 139–147.

Banerjee, A., Rapin, N., Bollinger, T., and Misra, V. (2017). Lack of inflammatory gene expression in bats: a unique role for a transcription repressor. Sci. Rep. *7*, 2232.

Banerjee, A., Nasir, J.A., Budylowski, P., Yip, L., Aftanas, P., Christie, N., Ghalami, A., Baid, K., Raphenya, A.R., Hirota, J.A., et al. (2020a). Isolation, sequence, infectivity, and replication kinetics of severe acute respiratory syndrome coronavirus 2. Emerg. Infect. Dis. *26*, 2054–2063.

Banerjee, A., Subudhi, S., Rapin, N., Lew, J., Jain, R., Falzarano, D., and Misra, V. (2020b). Selection of viral variants during persistent infection of insectivorous bat cells with Middle East respiratory syndrome coronavirus. Sci. Rep. *10*, 7257.

Banerjee, A., Zhang, X., Yip, A., Schulz, K.S., Irving, A.T., Bowdish, D., Golding, B., Wang, L.F., and Mossman, K. (2020c). Positive selection of a serine residue in bat IRF3 confers enhanced antiviral protection. iScience *23*, 100958.

Bastard, P., Rosen, L.B., Zhang, Q., Michailidis, E., Hoffmann, H.H., Zhang, Y., Dorgham, K., Philippot, Q., Rosain, J., Beziat, V., et al. (2020). Autoantibodies against type I IFNs in patients with life-threatening COVID-19. Science *370*, eabd4585.

Benjamini, Y., and Hochberg, Y. (1995). Controlling the false discovery rate: a practical and powerful approach to multiple testing. J. R. Stat. Soc. Ser. B (Methodological) *57*, 289–300.

Blanco-Melo, D., Nilsson-Payant, B.E., Liu, W.C., Uhl, S., Hoagland, D., Moller, R., Jordan, T.X., Oishi, K., Panis, M., Sachs, D., et al. (2020). Imbalanced host response to SARS-CoV-2 drives development of COVID-19. Cell *181*, 1036–1045.e9.

Bresnahan, W.A., Hultman, G.E., and Shenk, T. (2000). Replication of wild-type and mutant human cytomegalovirus in life-extended human diploid fibroblasts. J. Virol. *74*, 10816–10818.

Chen, W., Srinath, H., Lam, S.S., Schiffer, C.A., Royer, W.E., Jr., and Lin, K. (2008). Contribution of Ser386 and Ser396 to activation of interferon regulatory factor 3. J. Mol. Biol. *379*, 251–260.

Chen, X., Yang, X., Zheng, Y., Yang, Y., Xing, Y., and Chen, Z. (2014). SARS coronavirus papain-like protease inhibits the type I interferon signaling pathway through interaction with the STING-TRAF3-TBK1 complex. Protein Cell *5*, 369–381.

Couper, K.N., Blount, D.G., and Riley, E.M. (2008). IL-10: the master regulator of immunity to infection. J. Immunol. *180*, 5771–5777.

de Wit, E., van Doremalen, N., Falzarano, D., and Munster, V.J. (2016). SARS and MERS: recent insights into emerging coronaviruses. Nat. Rev. Microbiol. *14*, 523–534.

DeFilippis, V.R., Sali, T., Alvarado, D., White, L., Bresnahan, W., and Fruh, K.J. (2010). Activation of the interferon response by human cytomegalovirus occurs via cytoplasmic double-stranded DNA but not glycoprotein B. J. Virol. *84*, 8913–8925.

Ding, Z., Fang, L., Jing, H., Zeng, S., Wang, D., Liu, L., Zhang, H., Luo, R., Chen, H., and Xiao, S. (2014). Porcine epidemic diarrhea virus nucleocapsid protein antagonizes beta interferon production by sequestering the interaction between IRF3 and TBK1. J. Virol. *88*, 8936–8945.

Dong, E., Du, H., and Gardner, L. (2020). An interactive web-based dashboard to track COVID-19 in real time. Lancet Infect. Dis. *20*, 533–534.

Fehr, A.R., and Perlman, S. (2015). Coronaviruses: an overview of their replication and pathogenesis. Methods Mol. Biol. *1282*, 1–23.

Gordon, D.E., Jang, G.M., Bouhaddou, M., Xu, J., Obernier, K., White, K.M., O'Meara, M.J., Rezelj, V.V., Guo, J.Z., Swaney, D.L., et al. (2020). A SARS-CoV-2 protein interaction map reveals targets for drug repurposing. Nature *583*, 459–468.

Grimminger, F., and Schermuly, R.T. (2010). PDGF receptor and its antagonists: role in treatment of PAH. Adv. Exp. Med. Biol. *661*, 435–446.

Gu, Z., Eils, R., and Schlesner, M. (2016). Complex heatmaps reveal patterns and correlations in multidimensional genomic data. Bioinformatics *32*, 2847–2849.

Hadjadj, J., Yatim, N., Barnabei, L., Corneau, A., Boussier, J., Pere, H., Charbit, B., Bondet, V., Chenevier-Gobeaux, C., Breillat, P., et al. (2020a). Impaired type I interferon activity and exacerbated inflammatory responses in severe Covid-19 patients. medRxiv.

Hadjadj, J., Yatim, N., Barnabei, L., Corneau, A., Boussier, J., Smith, N., Pere, H., Charbit, B., Bondet, V., Chenevier-Gobeaux, C., et al. (2020b). Impaired type I interferon activity and inflammatory responses in severe COVID-19 patients. Science *369*, 718–724.

Harding, A.T., Heaton, B.E., Dumm, R.E., and Heaton, N.S. (2017). Rationally designed influenza virus vaccines that are antigenically stable during growth in eggs. mBio *8*, e00669ndash;17.

Hoagland, D.A., Moller, R., Uhl, S.A., Oishi, K., Frere, J., Golynker, I., Horiuchi, S., Panis, M., Blanco-Melo, D., Sachs, D., et al. (2021). Leveraging the antiviral type I interferon system as a first line of defense against SARS-CoV-2 pathogenicity. Immunity *54*, 557–570.e5.

Hung, I.F., Lung, K.C., Tso, E.Y., Liu, R., Chung, T.W., Chu, M.Y., Ng, Y.Y., Lo, J., Chan, J., Tam, A.R., et al. (2020). Triple combination of interferon beta-1b, lopinavir-ritonavir, and ribavirin in the treatment of patients admitted to hospital with COVID-19: an open-label, randomised, phase 2 trial. Lancet *395*, 1695–1704.

Hunt, S.E., McLaren, W., Gil, L., Thormann, A., Schuilenburg, H., Sheppard, D., Parton, A., Armean, I.M., Trevanion, S.J., Flicek, P., et al. (2018). Ensembl variation resources. Database (Oxford *2018*, bay119.

Janeway, C.A., Jr., and Medzhitov, R. (2002). Innate immune recognition. Annu. Rev. Immunol. *20*, 197–216.

Jassal, B., Matthews, L., Viteri, G., Gong, C., Lorente, P., Fabregat, A., Sidiropoulos, K., Cook, J., Gillespie, M., Haw, R., et al. (2020). The reactome pathway knowledgebase. Nucleic Acids Res. *48*, D498–D503.

Jiang, H.W., Zhang, H.N., Meng, Q.F., Xie, J., Li, Y., Chen, H., Zheng, Y.X., Wang, X.N., Qi, H., Zhang, J., et al. (2020). SARS-CoV-2 Orf9b suppresses type I interferon responses by targeting TOM70. Cell Mol Immunol *17*, 998–1000.

Katze, M.G., He, Y., and Gale, M., Jr. (2002). Viruses and interferon: a fight for supremacy. Nat. Rev. Immunol. *2*, 675–687.

Kawai, T., and Akira, S. (2006). Innate immune recognition of viral infection. Nat. Immunol. *7*, 131–137.

Koyama, S., Ishii, K.J., Coban, C., and Akira, S. (2008). Innate immune response to viral infection. Cytokine *43*, 336–341.

Krueger, F. (2019). Trim Galore. https://www.bioinformatics.babraham.ac.uk/projects/trim_galore/.

Lai, M.M. (1990). Coronavirus: organization, replication and expression of genome. Annu. Rev. Microbiol. *44*, 303–333.

Larabi, A., Devos, J.M., Ng, S.L., Nanao, M.H., Round, A., Maniatis, T., and Panne, D. (2013). Crystal structure and mechanism of activation of TANK-binding kinase 1. Cell Rep *3*, 734–746.

Lei, X., Dong, X., Ma, R., Wang, W., Xiao, X., Tian, Z., Wang, C., Wang, Y., Li, L., Ren, L., et al. (2020). Activation and evasion of type I interferon responses by SARS-CoV-2. Nat. Commun. *11*, 3810.

Leveille, S., Goulet, M.L., Lichty, B.D., and Hiscott, J. (2011). Vesicular stomatitis virus oncolytic treatment interferes with tumor-associated dendritic cell functions and abrogates tumor antigen presentation. J. Virol. *85*, 12160–12169.

Li, H. (2013). Aligning sequence reads, clone sequences and assembly contigs with BWA-MEM. arXiv.

Li, H., and Durbin, R. (2009). Fast and accurate short read alignment with Burrows-Wheeler transform. Bioinformatics *25*, 1754–1760.

Li, H., Handsaker, B., Wysoker, A., Fennell, T., Ruan, J., Homer, N., Marth, G., Abecasis, G., and Durbin, R.; Genome Project Data Processing, S. (2009). The sequence alignment/map format and SAMtools. Bioinformatics *25*, 2078–2079.

Lokugamage, K.G., Hage, A., de Vries, M., Valero-Jimenez, A.M., Schindewolf, C., Dittmann, M., Rajsbaum, R., and Menachery, V.D. (2020). Type I interferon susceptibility distinguishes SARS-CoV-2 from SARS-CoV. J. Virol. *94*, e01410ndash;20.

Long, Q.X., Tang, X.J., Shi, Q.L., Li, Q., Deng, H.J., Yuan, J., Hu, J.L., Xu, W., Zhang, Y., Lv, F.J., et al. (2020). Clinical and immunological assessment of asymptomatic SARS-CoV-2 infections. Nat. Med. *26*, 1200–1204.

Love, M.I., Huber, W., and Anders, S. (2014). Moderated estimation of fold change and dispersion for RNA-seq data with DESeq2. Genome Biol. *15*, 550.

Lu, X., Pan, J., Tao, J., and Guo, D. (2011). SARS-CoV nucleocapsid protein antagonizes IFN-beta response by targeting initial step of IFN-beta induction pathway, and its C-terminal region is critical for the antagonism. Virus Genes *42*, 37–45.

Lucas, C., Wong, P., Klein, J., Castro, T.B.R., Silva, J., Sundaram, M., Ellingson, M.K., Mao, T., Oh, J.E., Israelow, B., et al. (2020). Longitudinal analyses reveal immunological misfiring in severe COVID-19. Nature *584*, 463–469.

Lui, P.Y., Wong, L.Y., Fung, C.L., Siu, K.L., Yeung, M.L., Yuen, K.S., Chan, C.P., Woo, P.C., Yuen, K.Y., and Jin, D.Y. (2016). Middle East respiratory syndrome coronavirus M protein suppresses type I interferon expression through the inhibition of TBK1-dependent phosphorylation of IRF3. Emerg. Microbes Infect. *5*, e39.

Mandel, M., Harari, G., Gurevich, M., and Achiron, A. (2020). Cytokine prediction of mortality in COVID19 patients. Cytokine *134*, 155190.

Merico, D., Isserlin, R., Stueker, O., Emili, A., and Bader, G.D. (2010). Enrichment map: a network-based method for gene-set enrichment visualization and interpretation. PLoS One *5*, e13984.

Mesev, E.V., LeDesma, R.A., and Ploss, A. (2019). Decoding type I and III interferon signalling during viral infection. Nat. Microbiol. *4*, 914–924.

Minaker, R.L., Mossman, K.L., and Smiley, J.R. (2005). Functional inaccessibility of quiescent herpes simplex virus genomes. Virol. J. *2*, 85.

Nasir, J.A., Kozak, R.A., Aftanas, P., Raphenya, A.R., Smith, K.M., Maguire, F., Maan, H., Alruwaili, M., Banerjee, A., Mbareche, H., et al. (2020). A comparison of whole genome sequencing of SARS-CoV-2 using amplicon-based sequencing, random hexamers, and bait capture. Viruses *12*, 895.

Niemeyer, D., Zillinger, T., Muth, D., Zielecki, F., Horvath, G., Suliman, T., Barchet, W., Weber, F., Drosten, C., and Muller, M.A. (2013). Middle East respiratory syndrome coronavirus accessory protein 4a is a type I interferon antagonist. J. Virol. *87*, 12489–12495.

Noyce, R.S., Collins, S.E., and Mossman, K.L. (2009). Differential modification of interferon regulatory factor 3 following virus particle entry. J. Virol. *83*, 4013–4022.

Noyce, R.S., Taylor, K., Ciechonska, M., Collins, S.E., Duncan, R., and Mossman, K.L. (2011). Membrane perturbation elicits an IRF3-dependent, interferon-independent antiviral response. J. Virol. *85*, 10926–10931.

Paczkowska, M., Barenboim, J., Sintupisut, N., Fox, N.S., Zhu, H., Abd-Rabbo, D., Mee, M.W., Boutros, P.C., Drivers, P., et al.; Functional Interpretation Working G. (2020). Integrative pathway enrichment analysis of multivariate omics data. Nat. Commun. *11*, 735.

Park, A., and Iwasaki, A. (2020). Type I and type III interferons - induction, signaling, evasion, and application to combat COVID-19. Cell Host Microbe *27*, 870–878.

Patro, R., Duggal, G., Love, M.I., Irizarry, R.A., and Kingsford, C. (2017). Salmon provides fast and bias-aware quantification of transcript expression. Nat. Methods *14*, 417–419.

Pereda, R., Gonzalez, D., Rivero, H.B., Rivero, J.C., Perez, A., Lopez, L.D.R., Mezquia, N., Venegas, R., Betancourt, J.R., Dominguez, R.E., et al. (2020). Therapeutic effectiveness of interferon alpha 2b treatment for COVID-19 patient recovery. J. Interferon Cytokine Res. *40*, 578–588.

Perlman, S., and Netland, J. (2009). Coronaviruses post-SARS: update on replication and pathogenesis. Nat. Rev. Microbiol. *7*, 439–450.

Pilz, A., Ramsauer, K., Heidari, H., Leitges, M., Kovarik, P., and Decker, T. (2003). Phosphorylation of the Stat1 transactivating domain is required for the response to type I interferons. EMBO Rep. *4*, 368–373.

Pripp, A.H., and Stanisic, M. (2014). The correlation between pro- and anti-inflammatory cytokines in chronic subdural hematoma patients assessed with factor analysis. PLoS One *9*, e90149.

RCoreTeam, 2017. https://www.r-project.org.

Rebendenne, A., Valadao, A.L.C., Tauziet, M., Maarifi, G., Bonaventure, B., McKellar, J., Planes, R., Nisole, S., Arnaud-Arnould, M., Moncorge, O., et al. (2021). SARS-CoV-2 triggers an MDA-5-dependent interferon response which is unable to control replication in lung epithelial cells. J. Virol. *95*, e02415–e02420.

Reimand, J., Isserlin, R., Voisin, V., Kucera, M., Tannus-Lopes, C., Rostamianfar, A., Wadi, L., Meyer, M., Wong, J., Xu, C., et al. (2019). Pathway enrichment analysis and visualization of omics data using g:Profiler, GSEA, Cytoscape and EnrichmentMap. Nat. Protoc. *14*, 482–517.

Sadiq, M.A., Hanout, M., Sarwar, S., Hassan, M., Do, D.V., Nguyen, Q.D., and Sepah, Y.J. (2015). Platelet derived growth factor inhibitors: a potential therapeutic approach for ocular neovascularization. Saudi J. Ophthalmol. *29*, 287–291.

Sawicki, S.G., Sawicki, D.L., and Siddell, S.G. (2007). A contemporary view of coronavirus transcription. J. Virol. *81*, 20–29.

Schoggins, J.W. (2019). Interferon-stimulated genes: what do they all do? Annu. Rev. Virol. *6*, 567–584.

Schoggins, J.W., and Rice, C.M. (2011). Interferon-stimulated genes and their antiviral effector functions. Curr. Opin. Virol. *1*, 519–525.

Schulz, K.S., and Mossman, K.L. (2016). Viral evasion strategies in type I IFN signaling - a summary of recent developments. Front. Immunol. *7*, 498.

Shannon, P., Markiel, A., Ozier, O., Baliga, N.S., Wang, J.T., Ramage, D., Amin, N., Schwikowski, B., and Ideker, T. (2003). Cytoscape: a software environment for integrated models of biomolecular interaction networks. Genome Res. *13*, 2498–2504.

Shin, D., Mukherjee, R., Grewe, D., Bojkova, D., Baek, K., Bhattacharya, A., Schulz, L., Widera, M., Mehdipour, A.R., Tascher, G., et al. (2020). Papain-like protease regulates SARS-CoV-2 viral spread and innate immunity. Nature *587*, 657–662.

Siu, K.L., Yeung, M.L., Kok, K.H., Yuen, K.S., Kew, C., Lui, P.Y., Chan, C.P., Tse, H., Woo, P.C., Yuen, K.Y., et al. (2014). Middle east respiratory syndrome coronavirus 4a protein is a double-stranded RNA-binding protein that suppresses PACT-induced activation of RIG-I and MDA5 in the innate antiviral response. J. Virol. *88*, 4866–4876.

Soneson, C., Love, M.I., and Robinson, M.D. (2015). Differential analyses for RNA-seq: transcript-level estimates improve gene-level inferences. F1000Research *4*, 1521.

Steen, H.C., and Gamero, A.M. (2013). STAT2 phosphorylation and signaling. JAKSTAT *2*, e25790.

The Gene Ontology, C. (2019). The gene Ontology resource: 20 years and still GOing strong. Nucleic Acids Res. *47*, D330–D338.

Trouillet-Assant, S., Viel, S., Gaymard, A., Pons, S., Richard, J.C., Perret, M., Villard, M., Brengel-Pesce, K., Lina, B., Mezidi, M., et al. (2020). Type I IFN immunoprofiling in COVID-19 patients. J. Allergy Clin. Immunol. *146*, 206–208 e202.

Wickham, H. (2009). ggplot2: Elegant Graphics for Data Analysis (Springer-Verlag).

Wilk, A.J., Rustagi, A., Zhao, N.Q., Roque, J., Martinez-Colon, G.J., McKechnie, J.L., Ivison, G.T., Ranganath, T., Vergara, R., Hollis, T., et al. (2020). A single-cell atlas of the peripheral immune response in patients with severe COVID-19. Nat. Med. *26*, 1070–1076.

Xia, H., Cao, Z., Xie, X., Zhang, X., Chen, J.Y., Wang, H., Menachery, V.D., Rajsbaum, R., and Shi, P.Y. (2020). Evasion of type I interferon by SARS-CoV-2. Cell Rep *33*, 108234.

Xing, Y., Chen, J., Tu, J., Zhang, B., Chen, X., Shi, H., Baker, S.C., Feng, L., and Chen, Z. (2013). The

papain-like protease of porcine epidemic diarrhea virus negatively regulates type I interferon pathway by acting as a viral deubiquitinase. J. Gen. Virol. *94*, 1554–1567.

Xu, K., Cai, H., Shen, Y., Ni, Q., Chen, Y., Hu, S., Li, J., Wang, H., Yu, L., Huang, H., et al. (2020). Translation: Management of coronavirus disease 2019 (COVID-19): experience in Zhejiang province, China. Infect. Microbes Dis. *2*, 55–63.

Yamakawa, S., and Hayashida, K. (2019). Advances in surgical applications of growth factors for wound healing. Burns Trauma *7*, 10.

Yang, Y., Zhang, L., Geng, H., Deng, Y., Huang, B., Guo, Y., Zhao, Z., and Tan, W. (2013). The structural and accessory proteins M, ORF 4a, ORF 4b, and ORF 5 of Middle East respiratory syndrome coronavirus (MERS-CoV) are potent interferon antagonists. Protein Cell *4*, 951–961.

Yin, X., Riva, L., Pu, Y., Martin-Sancho, L., Kanamune, J., Yamamoto, Y., Sakai, K., Gotoh, S., Miorin, L., De Jesus, P.D., et al. (2021). MDA5 governs the innate immune response to SARS-CoV-2 in lung epithelial cells. Cell Rep *34*, 108628.

Zhou, P., Yang, X.L., Wang, X.G., Hu, B., Zhang, L., Zhang, W., Si, H.R., Zhu, Y., Li, B., Huang, C.L., et al. (2020a). A pneumonia outbreak associated with a new coronavirus of probable bat origin. Nature *579*, 270–273.

Zhang, Q., Bastard, P., Liu, Z., Le Pen, J., Moncada-Velez, M., Chen, J., Ogishi, M., Sabli, I.K.D., Hodeib, S., Korol, C., et al. (2020). Inborn errors of type I IFN immunity in patients with life-threatening COVID-19. Science *370*, 1–13.

Zhou, Z., Ren, L., Zhang, L., Zhong, J., Xiao, Y., Jia, Z., Guo, L., Yang, J., Wang, C., Jiang, S., et al. (2020b). Heightened innate immune responses in the respiratory tract of COVID-19 patients. Cell Host Microbe *27*, 883–890.e2.

STAR★METHODS

KEY RESOURCES TABLE

REAGENT or RESOURCE	SOURCE	IDENTIFIER
Antibodies		
Mouse anti-GAPDH	EMD Millipore	Catalogue number: AB2302; RRID: AB_10615768
mouse anti-SARS/SARS-CoV-2 N	ThermoFisher Scientific	Catalogue number: MA5-29981; RRID: AB_2785780
Human anti-SARS-CoV-2 N	GenScript	Catalogue number: A02039S; RRID: unavailable
rabbit anti-IFIT1	ThermoFisher Scientific	Catalogue number: PA3-848; RRID: AB_1958733
rabbit anti-beta-actin	Abcam	Catalogue number: ab8227; RRID: AB_2305186
rabbit anti-IRF3	Abcam	Catalogue number: ab68481; RRID: AB_11155653
rabbit anti-pIRF3-S396	Cell Signaling	Catalogue number: 4947; RRID: AB_823547
rabbit anti-TBK1	Abcam	Catalogue number: ab40676; RRID: AB_776632
rabbit anti-pTBK1-S172	Abcam	Catalogue number: ab109272; RRID: AB_10862438
rabbit anti-STAT1	Cell Signaling	Catalogue number: 9172; RRID: AB_2198300
rabbit anti-pSTAT1-Y701	Cell Signaling	Catalogue number: 9167; RRID: AB_561284
rabbit anti-STAT2	Cell Signaling	Catalogue number: 72604; RRID: AB_2799824
rabbit anti-pSTAT2-Y690	Cell Signaling	Catalogue number: 88410S; RRID: AB_2800123
donkey anti-rabbit 800	LI-COR Biosciences	Catalogue number: 926-32213; RRID: 621848
goat anti-mouse 680	LI-COR Biosciences	Catalogue number: 925-68070; RRID: AB_2651128
Rat anti-human FITC	BioLegend	Catalogue number: 410719; RRID: AB_2721575
Goat anti-mouse Texas Red-X	ThermoFisher Scientific	Catalogue number: T-6390; RRID: AB_2556778
Virus Strain		
SARS-CoV-2/SB3	Laboratory of Samira Mubareka	(Banerjee et al., 2020a)
VSV-GFP	Laboratory of Brian Lichty	(Leveille et al., 2011)
H1N1-mNeon	Laboratory of Matthew Miller	(Harding et al., 2017)
HSV-KOS-GFP	Laboratory of Karen Mossman	(Minaker et al., 2005)
Chemicals		
Poly(I:C)	InvivoGen	Cat#tlrl-pic
Lipofectamine	Invitrogen	Cat#L3000015
IFN-alpha 2	Sigma-Aldrich	SRP4594-100UG
ProLong Gold Antifade Mountant with DAPI	ThermoFisher Scientific	P36931
Poly(I:C)-Rhodamine	InvivoGen	Cat#tlrl-piwr
Critical commercial assays		
RNeasy Mini Kit	Qiagen	Cat No./ID: 74106
Drosophila Expression System	ThermoFisher Scientific	K5130-01

(*Continued on next page*)

Continued

REAGENT or RESOURCE	SOURCE	IDENTIFIER
iScript gDNA Clear cDNA synthesis kit	Bio-Rad	172-5035
Taqman Gene Expression assays	ThermoFisher Scientific	4331182
Ssofast EvaGreen supermix	Bio-Rad	1725201
Oligonucleotides		
IFNb1	ThermoFisher Scientific	catalog no. #4331182
IRF7	ThermoFisher Scientific	catalog no. #4331182
IFIT1	ThermoFisher Scientific	catalog no. #4331182
GAPDH	ThermoFisher Scientific	catalog no. #4331182
UpE	This study	SARS2 UpE F – ATTGTTGATGAGCCTGAAG and SARS2 UpE R – TTCGTACTCATCAGCTTG
GAPDH	Laboratory of Vikram Misra	(Banerjee et al., 2017)
Experimental models: Cell lines		
Vero E6	Laboratory of Samira Mubareka	(Banerjee et al., 2020a)
Calu-3 cells	ATCC	HTB-55
THF cells	Laboratory of Victor DeFilippis	(DeFilippis et al., 2010)
Drosophila S2 cells	ThermoFisher Scientific	K5130-01
Software and algorithms		
Prism software	GraphPad	https://www.graphpad.com
Image Studio	LI-COR Biosciences	https://www.licor.com/bio/image-studio/
Adobe Illustrator	Adobe	https://www.adobe.com/products/illustrator.html?promoid=PGRQQLFS&mv=other
BioRender	BioRender	https://biorender.com
R Scripts	This study	https://github.com/danieljrichard/Code-scripts-used-for-Banerjee-et-al.-2021
DESeq2 normalized transcript counts for all genes with RNA-Seq data	This study	Gene Expression Omnibus (GEO) database; NCBI GEO accession number GSE151513

RESOURCE AVAILABILITY

Lead contact

Further information and requests for resources and reagents should be directed to and will be fulfilled by lead contact, Dr. Karen Mossman (mossk@mcmaster.ca).

Materials availability

This study generated recombinant human IFNβ. The reagent will be made available on request as we are currently trying to secure a commercial partner to commercialize our recombinant proteins.

Data and code availability

The DESeq2 normalized transcript counts for all genes with RNA-Seq data, significant or otherwise, plus the raw sequencing FASTQ reads have been deposited into the Gene Expression Omnibus (GEO) database with NCBI GEO accession number GSE151513. R scripts can be accessed using https://github.com/danieljrichard/Code-scripts-used-for-Banerjee-et-al.-2021.

EXPERIMENTAL MODEL AND SUBJECT DETAILS

Cells and viruses

Vero E6 cells (African green monkey cells; ATCC) were maintained in Dulbecco's modified Eagle's media (DMEM) supplemented with 10% fetal bovine serum (FBS; Sigma-Aldrich), 1x L-Glutamine, and Penicillin/Streptomycin (Pen/Strep; VWR) (Banerjee et al., 2020a). Calu-3 cells (human male lung adenocarcinoma derived; ATCC) were cultured as previously mentioned (Aguiar et al., 2019). THF cells (human telomerase

life-extended cells; from Dr. Victor DeFilippis' lab, (Bresnahan et al., 2000; DeFilippis et al., 2010)) were cultured as previously mentioned (Banerjee et al., 2020c). *Drosophila* S2 cells (ThermoFisher Scientific) were cultured in Schneider's *Drosophila* medium supplemented with 10% FBS (Sigma-Aldrich) as recommended by the manufacturer and cells were incubated at 28°C. Sex of THF, Vero E6, and S2 cells are unknown as commercial vendors or collaborators did not have that information. Stocks of genetically engineered vesicular stomatitis virus (VSV-GFP) carrying a green fluorescent protein (GFP) cassette (Leveille et al., 2011; Noyce et al., 2011) were stored at −80°C. H1N1 (A/Puerto Rico/8/1934 mNeon – 2A-HA) stocks were obtained from Dr. Matthew Miller's laboratory (Harding et al., 2017). HSV-GFP stocks were generated and maintained as mentioned previously (Minaker et al., 2005). Clinical isolate of SARS-CoV-2 (SARS-CoV-2/SB3) was propagated on Vero E6 cells and validated by next-generation sequencing (Banerjee et al., 2020a). Virus stocks were thawed once and used for an experiment. A fresh vial was used for each experiment to avoid repeated freeze-thaws. VSV-GFP, HSV-GFP, and H1N1 infections were performed at a multiplicity of infection (MOI) of 1. SARS-CoV-2 infections were performed at MOIs of 0.1, 1, or 2. Experiments with SARS-CoV-2 were performed in a BSL3 laboratory, and all procedures were approved by institutional biosafety committees at McMaster University and the University of Toronto.

Subject details

Acute patient sera (<21 days from symptom onset) were acquired from moderate (hospital admission, but no ICU admission) and severe (ICU admission or death) cases of COVID-19 in Toronto, Canada, along with samples from uninfected, healthy individuals (see Table S4 for details). Work with patient sera was approved by the Sunnybrook Research Institute Research Ethics Board (amendment to 149-1994, March 2, 2020) (Nasir et al., 2020).

METHOD DETAILS

RNA-Seq

RNA was isolated from cells using RNeasy Mini kit (Qiagen). Sequencing was conducted at the McMaster Genomics Facility, Farncombe Institute at McMaster University. Sample quality was first assessed using a Bioanalyzer (Agilent), then enriched (NEBNext Poly(A) mRNA Magnetic Isolation Module; NEB). Library preparations were conducted (NEBNext Ultra II Directional RNA Library Prep Kit; NEB), and library fragment size distribution was verified (Agilent TapeSection D1000; Agilent). Libraries were quantified by qPCR, pooled in equimolar amounts, and qPCR and fragment size distribution verification were conducted again. Libraries were then sequenced on an Illumina HiSeq 1500 across 3 HiSeq Rapid v2 flow cells in 6 lanes (Illumina) using a paired-end, 2x50 bp configuration, with onboard cluster generation averaging 30.8M clusters per replicate (minimum 21.9M, maximum 46.0M).

Cytokine levels in COVID-19 patient sera

Sera were analyzed using a 48-plex human cytokine and chemokine array by the manufacturer (Evetechnologies). Samples with an observed cytokine concentration (pg/ml) below the limit of detection (OOR<) were floored to the lowest observed concentration for that cytokine. Average $\log_2$FC for moderate patients (n=10) versus healthy patients (n=5) and severe patients (n=10) versus healthy patients (n=5) was plotted using the pheatmap() R package (version 3.2.1) for all of the 48 cytokines. Cytokine expression levels were tested for significant differences via unpaired Student's t tests with Benjamini-Hochberg multiple testing correction using the *stats* R package (version 3.6.1).

Poly(I:C) transfection and IFN treatment

Calu-3 cells were mock transfected with 4 μl or 8 μl of lipofectamine 3000 (ThermoFisher Scientific) in Opti-MEM (ThermoFisher Scientific) only or transfected with varying concentrations of poly(I:C) (InvivoGen) or poly(I:C)-rhodamine (InvivoGen). Recombinant human IFNβ1 was generated using *Drosophila* Schneider 2 (S2) cells following manufacturer''s recommendation and by using ThermoFisher Scientific's *Drosophila* Expression system (ThermoFisher Scientific). Recombinant IFNβ1 was collected as part of the cell culture supernatant from S2 cells, and total protein was measured using Bradford assay. Total protein concentration was used for subsequent experiments. To demonstrate that S2 cell culture media did not contain non-specific stimulators of mammalian antiviral responses, we also generated recombinant green fluorescent protein (GFP) using the same protocol and used the highest total protein concentration (2 mg/ml) for mock-treated cells (Figure S3B). S2 cell culture supernatant containing GFP did not induce an antiviral response in human cells (Figure S3B). For VSV-GFP, HSV-GFP, and H1N1-mNeon infections, cells were

treated with increasing concentrations of IFNβ1 or GFP (control) containing cell culture supernatant. SARS-CoV-2-infected cells were treated with supernatant containing IFNβ1 or GFP. Commercially bought recombinant IFN-α2 (Sigma-Aldrich) was used for experiments that utilized IFN-α2.

Quantitative PCR

Calu-3 cells were seeded at a density of 3 x 10^5 cells/well in 12-well plates. Cells were infected with SARS-CoV-2 for 12 h. Twelve hours post incubation, mock-infected or infected cells were mock stimulated or stimulated with poly(I:C) or IFNβ for 6 h. RNA extraction was performed using RNeasy Mini Kit (Qiagen) according to manufacturer's protocol . Two hundred nanograms of purified RNA was reverse transcribed using iScript gDNA Clear cDNA Synthesis Kit (Bio-Rad). Quantitative PCR reactions were performed with TaqMan Universal PCR Master Mix (ThermoFisher Scientific) using pre-designed Taqman gene expression assays (ThermoFisher Scientific) for *IFNβ1* (catalog no. #4331182), *IRF7* (catalog no. #4331182), *IFIT1* (catalog no. #4331182), and *GAPDH* (catalog no. #4331182) according to manufacturer's protocol. Relative mRNA expression was normalized to *GAPDH* and presented as 1/ΔCt. To quantify SARS-CoV-2 genome levels, primers were designed to amplify a region (UpE) between *ORF3a* and *E* genes. Primer sequences used were SARS2 UpE F – ATTGTTGATGAGCCTGAAG and SARS2 UpE R – TTCGTACTCATCAGCTTG. qPCR to determine UpE levels was performed using SsoFast EvaGreen supermix (Bio-Rad) as previously described (Banerjee et al., 2017).

Agarose gel electrophoresis

UpE qPCR gene products were also run on agarose gels (Invitrogen) as previously mentioned to visualize qPCR amplicons (Banerjee et al., 2020b).

Immunoblots

Calu-3 cells were seeded at a density of 3 x 10^5 cells/well in 12-well plates. Cells were infected with SARS-CoV-2 at an MOI of 1. Control cells were sham infected. Twelve to twenty-four hours post incubation, cells were transfected or treated with poly(I:C) or IFNβ, respectively for indicated times. Cell lysates were harvested for immunoblots and analyzed on reducing gels as mentioned previously (Banerjee et al., 2020c). Briefly, samples were denatured in a reducing sample buffer and analyzed on a reducing gel. Proteins were blotted from the gel onto polyvinylidene difluoride (PVDF) membranes (Immobilon, EMD Millipore) and detected using primary and secondary antibodies. Primary antibodies used were as follows: 1:1000 mouse anti-GAPDH (EMD Millipore; Catalogue number: AB2302; RRID: AB_10615768), 1:1000 mouse anti-SARS/SARS-CoV-2 N (ThermoFisher Scientific; Catalogue number: MA5-29981; RRID: AB_2785780), 1:1000 rabbit anti-IFIT1 (ThermoFisher Scientific; Catalogue number: PA3-848; RRID: AB_1958733), 1:1000 rabbit anti-beta-actin (Abcam; Catalogue number: ab8227; RRID: AB_2305186), 1:1000 rabbit anti-IRF3 (Abcam; Catalogue number: ab68481; RRID: AB_11155653), 1:1000 rabbit anti-pIRF3-S396 (Cell Signaling; Catalogue number: 4947; RRID: AB_823547), 1:1000 rabbit anti-TBK1 (Abcam; Catalogue number: ab40676; RRID: AB_776632), 1:1000 rabbit anti-pTBK1-S172 (Abcam; Catalogue number: ab109272; RRID: AB_10862438), 1:1000 rabbit anti-STAT1 (Cell Signaling; Catalogue number: 9172; RRID: AB_2198300), 1:1000 rabbit anti-pSTAT1-Y701 (Cell Signaling; Catalogue number: 9167; RRID: AB_561284), 1:1000 rabbit anti-STAT2 (Cell Signaling; Catalogue number: 72604; RRID: AB_2799824), and 1:1000 rabbit anti-pSTAT2-Y690 (Cell Signaling; Catalogue number: 88410S; RRID: AB_2800123). Secondary antibodies used were: 1:5000 donkey anti-rabbit 800 (LI-COR Biosciences; Catalogue number: 926-32213; RRID: 621848) and 1:5000 goat anti-mouse 680 (LI-COR Biosciences; Catalogue number: 925-68070; RRID: AB_2651128). Blots were observed and imaged using Image Studio (LI-COR Biosciences) on the Odyssey CLx imaging system (LI-COR Biosciences).

Immunofluorescent microscopy

Calu-3 cells were infected with SARS-CoV-2 (MOI 1) for different times, followed by fixation in 10% neutral buffered formalin (Sigma) for 1 h. After fixation, cells were washed, permeabilized, and stained as mentioned previously (Banerjee et al., 2020b). Primary antibodies used were mouse anti-SARS/SARS-CoV-2 N (ThermoFisher Scientific; Catalogue number: MA5-29981; RRID: AB_2785780) and human anti-SARS-CoV-2 N (GenScript; Catalogue number: A02039S). Secondary antibodies used were goat anti-mouse Texas Red-X (ThermoFisher Scientific; Catalogue number: T-6390; RRID: AB_2556778) and rat anti-human FITC (BioLegend; Catalogue number: 410719; RRID: AB_2721575). Images were acquired using an EVOS M5000 imaging system (ThermoFisher Scientific).

Antiviral bioassay

THF cells were pre-treated or mock treated with recombinant human IFNβ, followed by VSV-GFP, HSV-GFP, or H1N1-mNeon infection at an MOI of 1. Infected cells were incubated at 37°C for 1 h with gentle rocking every 15 min. After 1 h, virus inoculum was aspirated, and Minimum Essential Medium (MEM) with Earle's salts (Sigma) containing 2% FBS and 1% carboxymethyl cellulose (CMC; Sigma) was added on the cells. Cells were incubated for 19 h at 37°C, and green fluorescent protein (GFP) or mNeon levels were measured using a typhoon scanner (Amersham, Sigma).

QUANTIFICATION AND STATISTICAL ANALYSIS

Transcript quantification and differential expression analysis

Sequence read quality was checked with FastQC (https://www.bioinformatics.babraham.ac.uk/projects/fastqc/), with reads subsequently aligned to the human reference transcriptome (GRCh37.67) obtained from the ENSEMBL database (Hunt et al., 2018) , indexed using the "index" function of Salmon (version 0.14.0) (Patro et al., 2017) with a k-mer size of 31. Alignment was performed using the Salmon 'quant' function with the following parameters: "-l A –numBootstraps 100 –gcBias –validateMappings". All other parameters were left to defaults. Salmon quantification files were imported into R (version 3.6.1) (RCoreTeam, 2017) using the tximport library (version 1.14.0) (Soneson et al., 2015) with the "type" option set to "'salmon." Transcript counts were summarized at the gene level using the corresponding transcriptome GTF file mappings obtained from ENSEMBL. Count data were subsequently loaded into DESeq2 (version 1.26.0) (Love et al., 2014) using the "DESeqDataSetFromTximport" function. In order to determine time/treatment dependent expression of genes, count data were normalized using the "estimateSizeFactors" function using the default "median ratio method" and output using the "counts" function with the "normalized" option.

For subsequent differential-expression analysis, a low-count filter was applied prior to normalization, wherein a gene must have had a count greater than five in at least three samples in order to be retained. Using all samples, this resulted in the removal of 12,980 genes for a final set of 15,760 used. Principal component analysis (PCA) of samples across genes was performed using the "vst" function in DESeq2 (default settings) and was subsequently plotted with the ggplot2 package in R (Wickham, 2009). Differential expression analyses were carried out with three designs: (a) the difference between infection/control status across all timepoints, (b) considering the effects of post-infection time (i.e. the interaction term between time and infection status), and (c) the difference between infection/control status at individual timepoints. (a) and (b) were performed using the "DESeq" function of DESeq2 using all samples, with results subsequently summarized using the "results" function with the "alpha" parameter set to 0.05; *p*-values were adjusted using the Benjamini-Hochberg FDR method (Benjamini and Hochberg, 1995), with differentially expressed genes filtered for those falling below an adjusted *p*-value of 0.05. For (c), infected/mock samples were subset to individual timepoints, with differential expression calculated using DESeq as described above. In addition, given the smaller number of samples at individual time points, differential-expression analysis was also performed with relaxation of the low-count filter described above, with results and p-value adjustments performed as above.

Viral transcript quantification

Paired-end sequencing reads were mapped to CDS regions of the SARS-CoV-2 genomic sequence (Assembly ASM985889v3 - GCF_009858895.2) obtained from NCBI, indexed using the "index" function of Salmon (version 0.14.0) (Patro et al., 2017) with a k-mer size of 31. Subsequently, reads were aligned using the Salmon "quant" function with the following parameters: "-l A –numBootstraps 100 –gcBias –validateMappings". All other parameters were left to defaults. Salmon quantification files were imported into R (version 3.6.1) (RCoreTeam, 2017) using the tximport library (version 1.14.0) (Soneson et al., 2015) with the 'type' option set to 'salmon'. All other parameters were set to default. Transcripts were mapped to their corresponding gene products via GTF files obtained from NCBI. Count data were subsequently loaded into DESeq2 (version 1.26.0) (Love et al., 2014) using the 'DESeqDataSetFromTximport' function. Principal component analysis (PCA) of samples across viral genes was performed using the 'vst' function in DESeq2 (default settings) and was subsequently plotted with the ggplot2 package in R (42) (Figure 1A). As viral transcript levels increased over time post infection, we first converted non-normalized transcript counts to a $\log_2$ scale and subsequently compared these across time points (Figure 1B and Table S1). To look at the changes in the expression of viral transcripts relative to total viral expression as a function of post-infection

time, normalized transcript counts were used to perform differential-expression analysis with DESeq2. Results and *p*-value adjustments were performed as described above.

In order to compare host/viral expression patterns, normalized transcript counts from infected samples were compared with either normalized or non-normalized viral transcript counts (from the same sample) across time points. For each viral transcript (n = 12), all host genes (n = 15,760, after filtering described above) were tested for correlated expression changes across matched infected samples (n = 18, across 5 time-points) using Pearson's correlation coefficient (via the cor.test function in R). Correlation test *p*-values were adjusted across all-by-all comparisons using the Benjamini-Hochberg FDR method, and gene-transcript pairs at adjusted $p < 0.05$ were retained. To account for possible effects of cellular response to plate incubation, viral transcript abundance was averaged at each time point and compared with host transcript abundance similarly averaged at each time point for non-infected samples; correlation testing was done all-by-all for n = 5 data points. Host genes that correlated with viral transcription in mock samples across time were removed from subsequent analyses; to increase stringency, mock correlation was defined using un-adjusted $p < 0.05$. Host genes were sorted by correlation coefficient (with any given viral transcript), with the top 100 unique genes retained for visualization. Normalized host transcript counts were z-score transformed per-gene using the 'scale' function in R, with normalized/un-normalized viral transcript counts similarly transformed per-transcript. Resulting z-score expression heatmaps were generated using the ComplexHeatmap library in R (version 2.2.0) (Gu et al., 2016). Heatmaps were generated for normalized/un-normalized viral transcript counts, given the different information revealed by absolute and relative viral expression patterns.

Viral genome mapping

Paired-end RNA-seq reads were filtered for quality control with Trim Galore! (version 0.6.4_dev) (Krueger, 2019) and mapped to the SARS-CoV-2 reference sequence (NC_045512.2) with the Burrow-Wheeler Aligner (Li and Durbin, 2009), using the BWA-MEM algorithm (Li, 2013). Output SAM files were sorted and compressed into BAM files using Samtools (version 1.10) (Li et al., 2009). Read coverage visualization was performed from within the R statistical environment (version 4.0.0) (RCoreTeam, 2017) using the "scanBam" function from the Rsamtools R package (version 1.32.0) to extract read coverage data and the ggplot2 R package (version 3.3.0) (Wickham, 2009) to plot read coverage histograms (using 300 bins across the SARS-CoV-2 sequence).

Cellular pathway enrichment analysis

To determine cellular pathways that were associated with differentially expressed genes (DEGs), the ActivePathways R (version 1.0.1) (Paczkowska et al., 2020) package was utilized to perform gene-set based pathway enrichment analysis. DEGs at each time point were treated as an independent set for enrichment analysis. Fisher's combined probability test was used to enrich pathways after *p*-value adjustment using Holm-Bonferroni correction. Pathways of gene-set size less than 5 and greater than 1000 were excluded. Only pathways enriched at individual time-points were considered for downstream analysis; pathways enriched across combined timepoints as determined by ActivePathways Brown's *p*-value merging method were filtered out. Visualization of enriched pathways across timepoints was done using Cytoscape (version 3.8.0) (Shannon et al., 2003) and the EnrichmentMap plugin (version 3.2.1) (Merico et al., 2010), as outlined by Reimand et al. (Reimand et al., 2019). Up-to-date Gene-Matrix-Transposed (GMT) files containing information on pathways for the Gene Ontology (GO), Molecular Function (MF), GO Biological Process (BP) (The Gene Ontology, 2019), and REACTOME (Jassal et al., 2020) pathway databases were utilized with ActivePathways. Only pathways that were enriched at specific time points were considered. Bar plots displaying top ActivePathway GO terms and REACTOME enrichments for infection versus mock were plotted using the ggplot2 R package (version 3.2.1) for 1-, 2-, 3-, and 12-h time points. Zero and 6-h time points were omitted due to a lack of sufficient numbers of differentially expressed genes required for functional enrichment analysis.

Statistical analysis

Statistical analyses for RNA-seq data were performed in R and are mentioned under the respective RNA-seq analyses sections. All other statistical calculations were performed in GraphPad Prism (version 8.4.2; www.graphpad.com). Significance values and statistical tests used are indicated in the figures and figure legends. *p**<0.05, **<0.01, ***<0.001, and ****<0.0001.